Fall 2014

Development and characterization of spiral additions in a ceramic matrix

Andrea Lynn Els

Follow this and additional works at: https://scholarsmine.mst.edu/masters_theses

Part of the Materials Science and Engineering Commons

Department:

Recommended Citation

Els, Andrea Lynn, "Development and characterization of spiral additions in a ceramic matrix" (2014). *Masters Theses*. 7326.

https://scholarsmine.mst.edu/masters_theses/7326

DEVELOPMENT AND CHARACTERIZATION OF SPIRAL ADDITIONS IN A CERAMIC MATRIX

by

ANDREA LYNN ELS

A THESIS

Presented to the Faculty of the Graduate School of the

MISSOURI UNIVERSITY OF SCIENCE AND TECHNOLOGY

In Partial Fulfillment of the Requirements for the Degree

MASTER OF SCIENCE IN CERAMIC ENGINEERING

2014

Approved by

Dr. Jeremy Watts, Advisor
Dr. Gregory E. Hilmas
Dr. William G. Fahrenholtz

PUBLICATION THESIS OPTION

The sections of this thesis are formatted for publication. The Introduction and Literature Review sections provide information about the thesis topic as well as summarize the manuscripts. Paper I and II, pages 18-35 and 43-53 respectively, are formatted for publication in Ceramics International. The thesis concludes with an overall summary and suggestions for future work.

ABSTRACT

A novel spiral architecture was formed using titanium diboride and silicon carbide ceramics as either the spiral or matrix phase. Particulate composites with the same compositions were fabricated to compare to the materials in this study. Spiral additions were formed using powder loaded polymers followed by a single and/or multi-filament co-extrusion. For 25 vol% SiC spiral additions to TiB_2, boron nitride was added to the SiC spiral to alter the bonding at the interface and reduce thermal residual stresses. All samples were hot-pressed to near full density at 1980 °C. Hot pressed multi-filament co-extrusion of 2.4 mm / 1 mm resulted in the smallest, consistent spirals ~50 μm in diameter. For the SiC spirals in TiB_2 study, the room temperature flexure strength was 193 ± 17 MPa, with the particulate composite being 488 ± 45 MPa. The fracture toughness for the spiral material was as high as 7.5 ± 0.6 MPa·$m^{1/2}$ with the particulate composite being 5.3 ± 0.4 MPa·$m^{1/2}$. Spiral length was studied with TiB_2 spirals in a SiC matrix. The resulting average room temperature flexure strength was 313 ± 11 MPa and 417 ± 41 MPa for spiral and monolithic samples, respectively. Fracture toughness was increased from 4.2 ± 0.2 MPa·$m^{1/2}$ for the monolithic to 6.2 ± 0.4 MPa·$m^{1/2}$ with the addition of spirals. The higher fracture toughness is a result of crack deflection in and around the spiral inclusions. Wear testing resulted in a loss of 1.1 mm^3 and 3.3 mm^3 per 6000 revolutions for monolithic and uniaxial specimens, respectively. While more wear was observed, the strength of the uniaxial samples after wear increased 16% whereas monolithic strength decreased 18%.

ACKNOWLEDGMENTS

First of all, I would like to thank my advisors Drs. Jeremy Watts, Greg Hilmas and Bill Fahrenholtz. Without your guidance, encouragement and sense of humor I am not sure I would have made it.

I would also like to take the opportunity to thank the University of Missouri Research Board for funding my research and giving me the ability to further my education.

I would like to also acknowledge ALL of the people who have called McNutt 307 their home away from home the last five years. To those present in my early years, Harlan, Jeremy, Greg, and Maryam, thank you for giving me the unique opportunities that influenced my decision to attend graduate school. To those present in my later years, Ben, Devon, Ryan, Greg, Jason, Derek, thank you for all the brainstorming, troubleshooting, and bull sessions, but most of all your friendship.

This list of acknowledgements would not be complete without the family and friends in my life. Brian, thank you for all the formatting help! Also, thank you for all the unique experiences the last few years that have truly changed who I am. Susan, Emilie, Bryan, and BJ thanks for all the advice and life lessons you have taught me all these years, the ones only siblings can teach! Last but definitely not least, Mom and Dad, your endless support never ends and I cannot even begin to express my gratitude. Thank you for encouraging me to explore my horizons and providing me with the tools to get to where I am today.

TABLE OF CONTENTS

LIST OF ILLUSTRATIONS

LIST OF TABLES

1. INTRODUCTION

With the improvement of metal alloys, the machinery to shape and cut these new alloys must too improve. In order to accommodate the high temperature demands (up to ~1000°C), SiC and TiB_2 are good candidates. Both materials have advantageous properties with respect to high speed machining applications including high melting temperature (2700-3200°C), high strength (300-420 MPa), high hardness (20-27 GPa), high thermal conductivity (70-120 $W \cdot m^{-1} K^{-1}$) and are largely chemically inert.[1,2]

With machining tools, fracture toughness is a key design factor when considering material choices. Many toughening mechanisms have been researched concerning ceramics. Previous research on toughening SiC and TiB_2 composites have included particulate, whisker or fiber additions, or annealing.[3-6] Engineered microstructures have been another method used to impart toughness and have been researched in other ceramic systems. One example is fibrous monoliths which consist of a hard, strong core material surrounded by a weaker shell material. The weaker shell allows crack propagation perpendicular to the applied force while the core retains the load. The core-shell structure can be produced using co-extrusion techniques to create a uniform cross-section of the core –shell geometry.[7]

One consequence to producing composites of varying materials is the generation of thermal residual stresses. This issue has been studies for certain ceramic systems. Modeling of the thermal residual stresses formed during cooling of ZrB_2-SiC composites has been performed with various geometries of SiC additions such as round, square,

hexagonal, peanuts and spirals.[8] The round geometry was used as a standard best comparable to a particulate addition. The peanut geometry was pursued after observing the hexagonal results where an increase in residual stresses was observed near corners of hexagons, but not along the flat sides. The peanuts were modeled such that the convex side of one was adjacent to the concave side of another. This resulted in a reduced magnitude of residual stress field with these additions. The modeling of the spiral additions resulted in the least amount of difference in the tensile and compressive stresses of all the geometries modeled.

The current study focused on modifying current co-extrusion methods to create unique spiral geometries. Although co-extrusion has most commonly been used for axisymmetric or co-axial geometries, previous studies have indicated that the spiral architecture can be achieved.[9] The spiral inclusions were then incorporated into a ceramic matrix to determine the mechanical properties and how they compare to simple particulate composites. The strength, fracture toughness and wear properties of these materials were then studied to best characterize them in relation to potential machining applications.

2. LITERATURE REVIEW

2.1 MECHANICAL PROPERTIES

2.1.1 Strength. The strength of a material is dependent on the atomic bonding of the structure. The amount of energy required to break a chemical bond is equal to the energy under the force-distance curve in Figure 2.1.[10] The atoms in the illustration have a preferred separation distance x_o at which the potential energy is at its lowest point. As a tensile force is applied the distance between the two atoms is increased. Once the distance at which the bond energy has been exceeded is reached, the atoms no longer act on one another and the bond has been broken. This distance can be related to a sine wave of the idealized force displacement curve with Equation 1. Where λ is the atomic spacing change, x is the displacement and P_c is equal to the cohesive force.[10]

$$P = P_c sin\left(\frac{\pi x}{\lambda}\right) \tag{1}$$
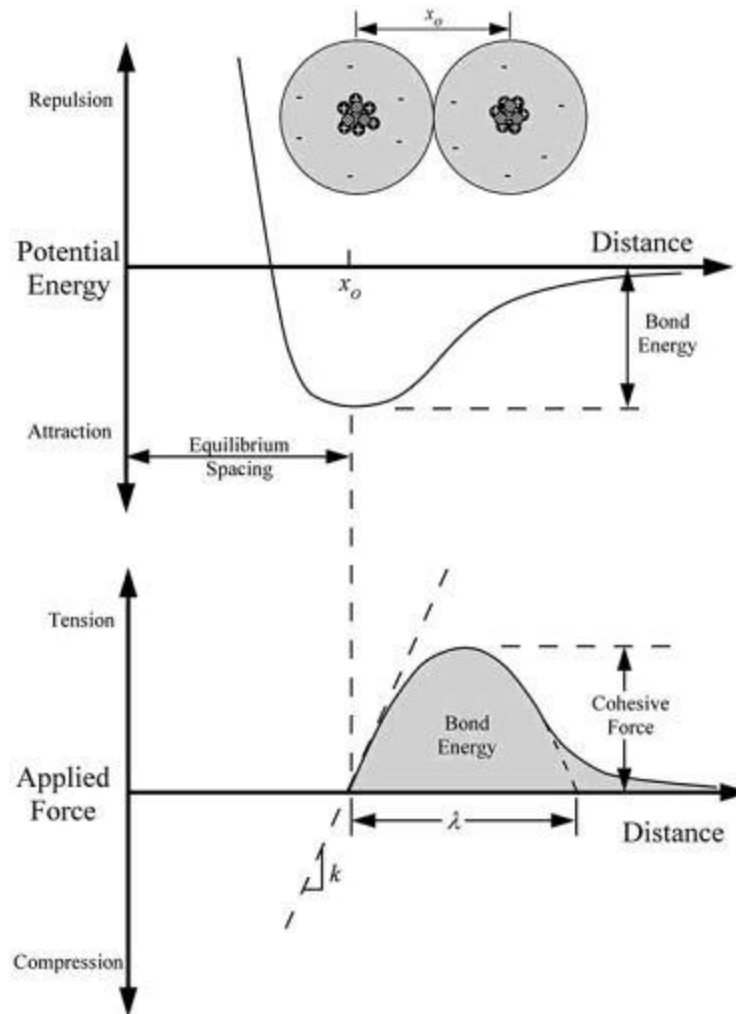
Figure 2.1. Potential bond energy between two atoms (top) and the energy required to overcome that bond energy (bottom).[10]

The cohesive force, proposed by Orowan, which follows an approximate half sine function can be used to derive Equation 2[11] where E is the elastic modulus, γ is the fracture surface energy and a_o is the equilibrium separation of atoms.

$$\sigma_{Th} \approx \left(\frac{E\gamma}{a_o}\right)^{1/2} \tag{2}$$

However, this model does not account for flaws in a material, thus relating to single crystal materials or in the best case, a high purity fiber. For polycrystalline

materials, however, this model is unrealistic. For example approximate theoretical strength values for TiB$_2$ and SiC are 180 GPa and 132 GPa, respectively. Griffith realized this and modified this equation with the consideration of flaws in the material to form Equation 3.[11] Where π is the geometrical crack constant which can vary and is subject to the crack geometry which will be discussed in a later section, and c is the critical flaw size.

$$\sigma_f = \left(\frac{2E\gamma}{\pi c}\right)^{1/2} \tag{3}$$

In order to measure the strength of ceramic materials, flexure testing is most commonly used due to cost and convenience. A detailed description of this test method for ceramics can be found in ASTM C1161.[12]

2.1.2 Fracture Toughness. Irwin continued the study of flaws in brittle materials, considering the stress field around cracks. At the tip of a crack the stresses can be defined in polar coordinates, in which the direction of the loading is considered. There are three different ways, or modes of loading to test a material; tension, in-plane shear and out-of-plane shear, illustrated in Figure 2.2. Mode I, tension is most commonly used to test materials, where the load is applied normal to the crack plane. The stress intensity factor, K, for these materials can be determined for either loading method or specimen geometry. With K_I being the stress intensity factor in Mode I failure. The point at which the stress causes the flaw to propagate becomes the critical stress intensity factor, K_{IC}, which can be considered a measure of the fracture toughness

of a material. Once a crack in a material has been initiated, fracture toughness is a measure of a materials ability to resist the propagation of the crack.
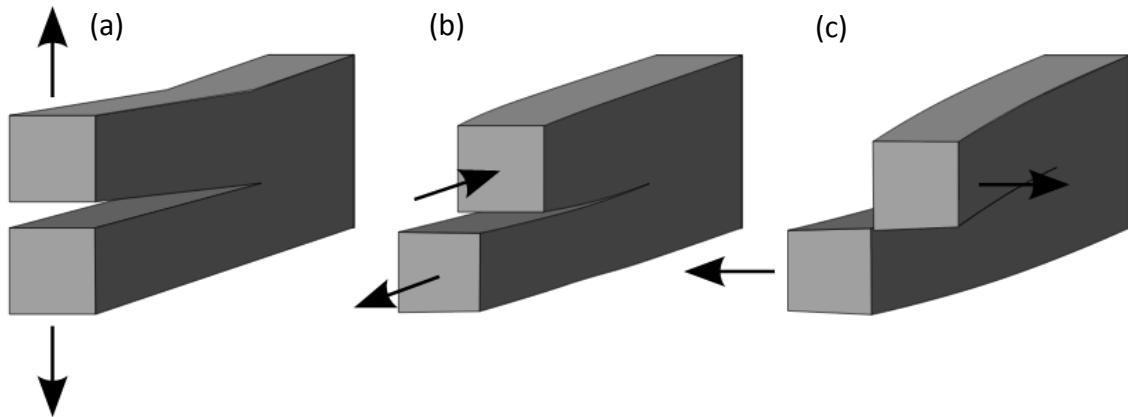
Figure 2.2. Failure modes of materials (a) tension (b) in-plane shear and (c) out-of-plane shear

While there are many methods for determining fracture toughness, four main techniques are generally used to measure the fracture toughness of ceramics: indirect crack, direct crack, chevron and pre-cracked beam method (straight notch), but each method has numerous variations. For the direct crack method, a Vickers indent is made on the surface of the material and the length of the radial/median cracks that grow from the corners of the indent are measured. Using Equation 4,[13] K_{IC} can be calculated, where ξ is an empirical constant (0.016 ± 0.004). Chevron and straight notch bar cross-sections are illustrated in Figure 2.3. The gray area indicates the area that is cut away, introducing a known flaw size into the sample. The notch is tested in tension via either 3 or 4-point bending. Using the maximum load with stable growth and dimensions of the

flaw, K_{IC} can be calculated. Methods for specimen preparation, testing and data analysis are detailed in ASTM C1421-10.[14]

$$K_{\mathrm{IC}} = \xi \left(\frac{E}{H}\right)^{\frac{1}{2}} \left(\frac{P}{c^{\frac{3}{2}}}\right) \tag{4}$$
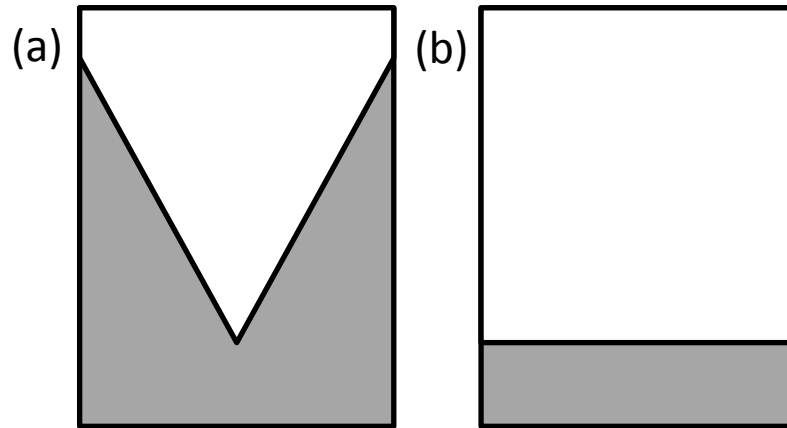
Figure 2.3. Schematic of (a) Chevron notch and (b) straight notch cross-sections where the gray area is that of the material that is cut away

Relating fracture toughness, K_{IC}, back to the flexure strength gives Equation 5[13] where Y is the stress intensity factor dependent on the geometry of a crack and K_{IC} relates to twice the elastic modulus times the fracture surface energy, γ. If Y is known, the critical flaw size, c, can be calculated, given the experimental measurements of fracture toughness and flexure strength.

$$K_{IC} = \sigma_f Y c^{1/2} \tag{5}$$

Griffith proposed several stress intensity factors, Y, for different crack geometries[13]: through thickness internal crack ($Y=\sqrt{\pi}$), through thickness surface crack ($Y=1.12\sqrt{\pi}$), internal circular 'penny' crack ($Y=2/\sqrt{\pi}$), and through thickness internal crack in a finite width body (Equation 6)[13] where w is the width of the specimen. If c is much less than w, the equation equals that of the geometry for a through thickness internal crack ($Y=\sqrt{\pi}$), but as c gets closer to w, Y increases to infinity.

$$Y = \left[\frac{2w}{c} tan\left(\frac{\pi c}{2w}\right)\right]^{1/2} \tag{6}$$

2.2 FIBROUS MONOLITHS & CO-EXTRUSION

2.2.1 Processing. Fibrous monoliths (FM) were originally fabricated using a piece of cotton thread drawn through a ceramic paste to coat the thread by Coblenz.[15] The threads were drawn through an alumina paste, dried, then through a titania coating to produce the cellular structure. Coblenz cut and laid up the fibers uniaxially and pressed them. After binder burnout to remove the organics from the powder processing and the cotton threads, the parts were isopressed to remove voids created from burnout and sintered. The samples tested in four-point flexure testing resulted in graceful failure, which was the first demonstration of increased work of fracture that did not include manufactured fibers. From this development in 1988, two different methods of FM fabrication were researched at the University of Michigan, dry spinning or melt spinning of the core material followed by a coating for the cell,[16] and co-

extrusion.[17] To dry spin the material, ceramic powders to make up the core were blended with a polymer, ethyl methacrylate (EMA), and solvent, methyl ethyl ketone (MEK). The components were milled and the majority of the solvent was evaporated to create a viscous slurry, which was extruded into a drying chamber to complete evaporation, resulting in fibers. Melt spinning incorporates the ceramic powders in a thermoplastic which was formed into a feedrod and heated to be extruded. Both techniques used dip coating to apply the boundary material to the cell fibers.

The second method, co-extrusion, was patented by the researchers at the University of Michigan[7] and involves combining the ceramic powder with a thermoplastic binder. The harder core material is pressed to a slightly smaller version of the extrusion feedrod and the cell material is pressed into c-shaped shells that fit around the smaller feedrod, illustrated in Figure 2.4. With the shells around the core, the feedrod can then be extruded. After extrusion, the compact must undergo a binder burnout to remove the polymer before sintering. As the binder makes up ~50 vol% of the compact, burnout often takes days, compared to hours for most ceramics that are processed with much lower volume fractions of organic additives.
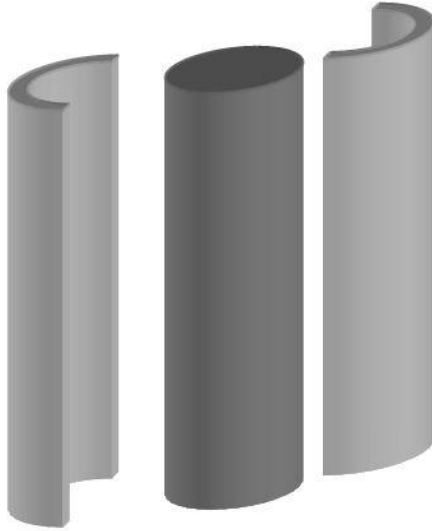
Figure 2.4. Schematic of core and shell.

2.2.2 Properties. The core and shell structure of FMs allows the material to exhibit graceful failure rather than catastrophic failure typical with ceramics as exhibited in Figure 2.5. The load displacement curve exhibits multiple instances where load is maintained even after the initiation or propagation of a crack. This becomes beneficial for structural applications that the FM's will be able to sustain some damage and still support significant load prior to failure.
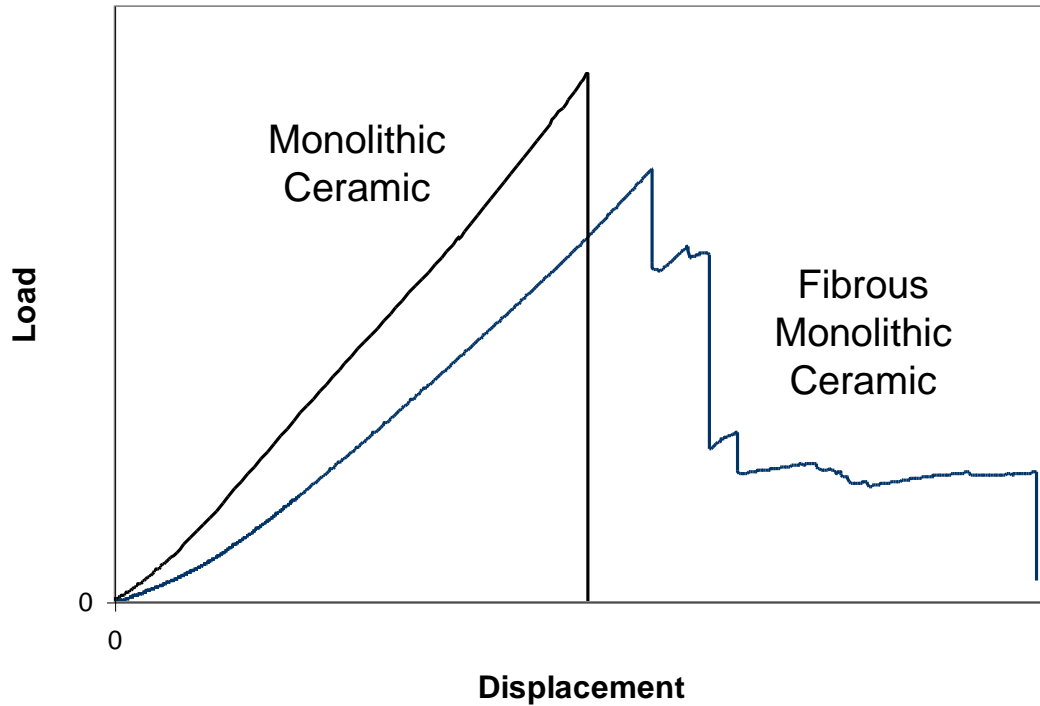
Figure 2.5. Load displacement curves highlight the difference between flexure behavior of monolithic and fibrous monolithic ceramics.[18]

However, not all fibrous monoliths exhibit improved fracture behavior. Zimmermann et al.[19] created FMs with a core material of ZrB_2 – 30 vol% SiC and shell of graphite – 30 vol% ZrB_2. This composition failed catastrophically like a typical monolithic specimen. The ZrB_2 content in the graphite shell had to be reduced to 15 vol% before graceful failure was observed. Figure 2.6 illustrates the fracture energies of cell boundary/cell ratio from Zimmermann's work plotted with Dunder's α-parameter for different percentages of graphite in the cell boundaries. The line is based on He and Hutchinson's[20] work which indicates the critical ratio threshold which is expected to result in crack deflection which is on or below the line.
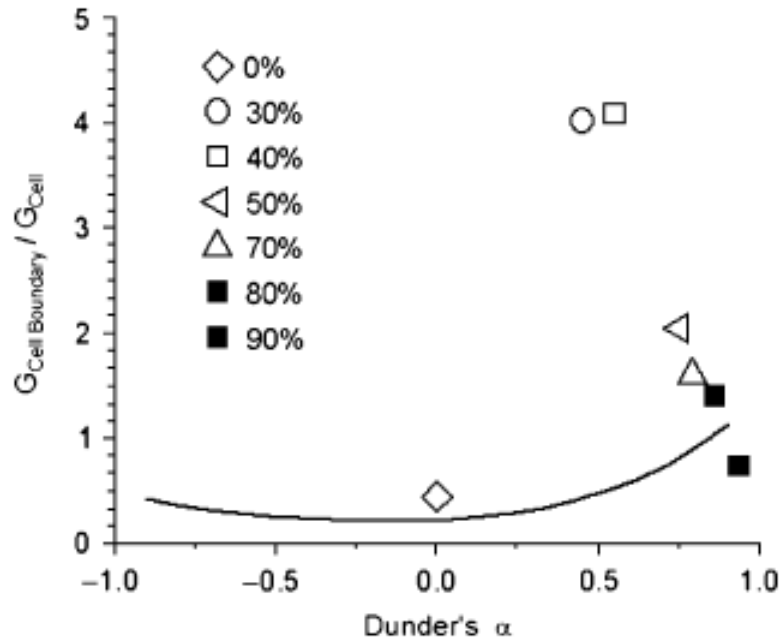
Figure 2.6. Ratio of cell boundary/cell material against Dunder's α-parameter. Plotted based on He and Hutchinson's 1989 work where crack deflection is expected to occur below the line.[20]

Research at the University of Michigan investigated a silicon carbide/boron nitride FM system that also underwent heat treatments.[21] The SiC cell fibers were dry spun to ~150-200 μm filament and coated in a BN slurry for the boundary phase ~2-25 μm thick. When tested in 4-point flexure, graceful failure was exhibited and when indented, long cracks were not able to form due to interactions with the BN cell boundary. Heat treatments were performed with these materials for 10 hours in air at 1200, 1300, 1400 and 1500°C to determine the effect of oxidation. The samples exhibited little to no effect from the oxidation, with little change in strength or graceful failure behavior for all samples.

The researchers at Michigan also studied the alumina/nickel system, utilizing the ductility of Ni as the cell boundary for the alumina cell.[22] The alumina cell was dry spun to a diameter of ~175 μm and dip coated with NiO slurry. Two sets of samples were fabricated, 3 and 8 vol% Ni cell boundary. The 3 vol% Ni boundary resulted in catastrophic failure, but the 8 vol% exhibited graceful failure. When indented it also exhibited crack blunting and arresting behavior.

2.3 TITANIUM DIBORIDE AND SILICON CARBIDE CERAMIC COMPOSITES

2.3.1 Particulate Composites Processing. TiB_2 and SiC ceramics are most simplistically processed by combining the individual powders with sintering additives, such as B_4C and C. The powders can then be either pressurelessly sintered or hot-pressed. B_4C and C are necessary for densification of these materials as shown by Basu[23] and Baik[24] for TiB_2 and Prochazka[25] and Greskovich[26] for SiC, to name a few.

There are six mechanisms by which sintering occurs (illustrated in Figure 2.7): (1) surface diffusion, in which atoms move along the surface of the particle due to higher lattice energy; (2) lattice diffusion of atoms from the surface to the lower energy region of the neck; (3) vapor transport in which the atoms vaporize from the surface of the atom to condense at the neck of the two atoms and grain boundary; (4) grain boundary diffusion; (5) lattice diffusion from the grain boundary; and (6) plastic flow caused by dislocation motion. While there are six different mechanisms, only mechanisms four, five, and six result in densification. Mechanisms one, two, and three result in

microstructural changes which form the neck of the two grains and contribute to grain

coarsening.[27]

Mechanisms
1. Surface diffusion
2. Lattice diffusion
   (from the surface)
3. Vapor transport
4. Grain boundary diffusion
5. Lattice diffusion (from
   the grain boundary)
6. Plastic flow
   (by dislocation motion)

Non-densifying mechanisms 1, 2, and 3 produce microstructural change without causing shrinkage

Densifying mechanisms 4, 5, and 6 remove material from the grain boundary region leading to shrinkage

Figure 2.7. The six mechanisms of sintering: (1) surface diffusion, (2) lattice diffusion from the surface, (3) vapor transport, (4) grain boundary diffusion, (5) lattice diffusion from the grain boundary, and (6) plastic flow by dislocation motion.[27]

Baik specifically looked into the effect of oxygen contamination on the

densification of TiB_2. His research showed the presence of excess oxygen led to

increased grain growth and resulted in entrapped porosity. The density trends also

indicated the dominating densification mechanism with excess oxygen to be vapor

transport, rather than grain boundary diffusion. The removal of surface oxides from TiB_2

can follow the carbothermal Reaction 2 and 3 as well as the evaporation of liquid boria

(B_2O_3) in Reaction 1.

$$B_2O_{3\,(l)} \rightarrow B_2O_{3\,(g)} \tag{1}$$

$$B_2O_{3\,(l)} + 3C \rightarrow 2B + 3CO_{(g)} \tag{2}$$

$$2TiO_2 + B_4C + 3C \rightarrow 2TiB_2 + 4CO \tag{3}$$
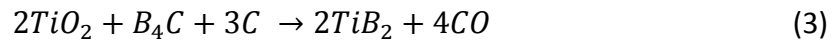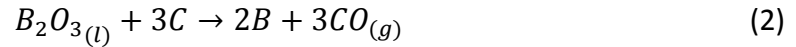
The equilibrium vapor pressures for reactions 2 and 3 are plotted versus temperature in Figure 2.8 where the solid lines represent the equilibrium vapor pressures of B_2O_3 and CO as a function of temperature and the shaded region represents a common processing window of vacuum pressures. The carbothermal reaction becomes favorable at ~900°C and the boria that has not been reduced will begin to evaporate at ~ 1250°C. These reactions are critical in order to maximize densification of TiB_2 by the removal of surface oxides.

In order to densify SiC, B_4C and C are also used. Prochazka *et al.* were the first to note the increased sinterability of SiC with B_4C and C additions. The authors also noted that without enough B, little densification occurred. The required amount of B added needed to exceed the solubility limit of B in SiC. The optimal limit was found to be ~3 wt%. SiC has a similar reaction as TiB_2 for the removal of surface oxides (Reaction 4). In addition Kang *et al.*[28] determined that B_4C also acts as a pinning agent to slow grain coarsening in TiB_2 ceramics, aiding in densification and resulting in nominally small, equiaxed grains.

$$SiO_2 + 3C \rightarrow SiC + 2CO_{(g)} \tag{4}$$
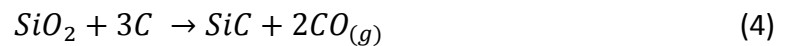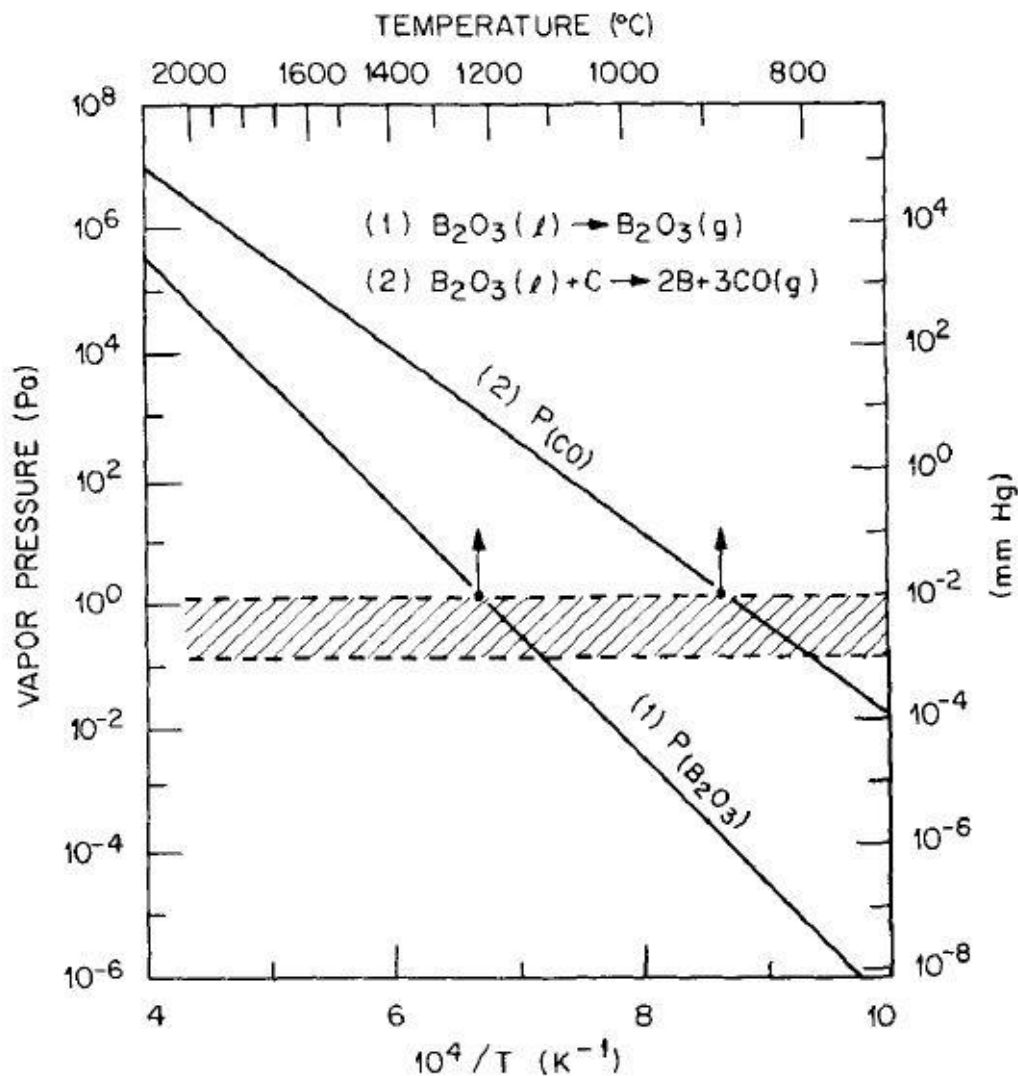
Figure 2.8. Equilibrium vapor pressure with temperature of (1) B_2O_3 and (2) CO for reactions 1 and 2 as listed above.

2.3.2 Properties of TiB₂ and SiC Composites TiB_2 is strong (400-425 MPa),

tough (5.8-6.2 MPa·m$^{1/2}$), thermally conductive (70-96 W/m·K), hard (Vickers hardness

22-26 GPa) and chemical stable.[29-32] These properties make TiB_2 an ideal candidate for

many applications including cutting tools, wear resistant parts and armor materials, just

to name a few.[23,29]

SiC also has many favorable attributes such as strength (305-412 MPa), hardness (20-27 GPa), thermal conductivity (105-123 W m^{-1} K^{-1}), and chemical inertness.[33-35] These properties make it a candidate for many applications, like TiB_2. Combinations of the two materials can be made such that their beneficial properties are minimally impacted while improving both strength and toughness. The combination of TiB_2 and SiC has been researched extensively for various ratios of the two materials. King *et al.* studied the hardness and fracture toughness through the concentration range of 100 vol.% SiC to 100 vol.% TiB_2. The highest hardness measured after that of 100 vol% SiC of 27.8 ± 1.1 GPa was that of SiC-25 vol% TiB_2 at 27.2 ± 1.5 GPa. The highest fracture toughness was measured from the 40 vol% TiB_2 sample with a K_{IC} of 6.2 ± 1.0 MPa·m$^{1/2}$. These materials exhibited a hardness/toughness tradeoff with their intersection at a concentration of ~35 vol.% TiB_2 in SiC.[32]

Chen *et al.* measured strength, hardness and fracture toughness of pressurelessly sintered TiB_2-SiC and found with increasing SiC content the strength increased and the hardness decreased. There was no clear change in the fracture toughness however, until the sample was 100 mol.% SiC.[36] Cho *et al.*[37] studied a range in SiC-TiB_2 composites; however, they studied the effects of annealing and microstructure design. Regardless of composition, with increasing annealing time the fracture toughness increased while flexure strength decreased. These effects were due to the grain coarsening during annealing.[37]

PAPER

I. PROCESSING AND PROPERTIES OF TIB₂-SIC AND TIB₂-SIC/BN CERAMICS CONTAINING A SPIRAL ARCHITECTURE

Andrea Els, Jeremy Watts, Greg Hilmas, William Fahrenholtz

ABSTRACT

A novel ceramic architecture consisting of a titanium diboride matrix containing 25 vol.% of silicon carbide spirals was processed using a powder loaded thermoplastic polymer followed by single or multi-filament co-extrusion. Boron nitride was also added to the silicon carbide spiral phase to alter the thermal expansion coefficient and reduce the mismatch between the phases. Spiral containing compositions, and a monolithic TiB$_2$-SiC composition, were hot pressed to near full density at 1980°C. After hot pressing, single filament co-extrusion resulted in SiC spirals ~180 µm in diameter, randomly dispersed in a TiB$_2$ matrix. Multi-filament co-extrusion resulted in a more consistent architecture, with spirals ~50 µm in diameter. The room temperature flexural strength for the multi-filament co-extrusion spiral compositions was 193 ± 17 MPa, compared to 488 ± 45 MPa for the monolithic ceramic. The fracture toughness of the compositions containing spirals was as high as 7.5 ± 0.6 MPa·m$^{1/2}$ with the monolithic material having a toughness of 5.3 ± 0.4 MPa·m$^{1/2}$. The boost in fracture toughness was due to significant crack deflection within and around the spiral inclusions.

INTRODUCTION

Titanium diboride (TiB_2), one of a family of transition metal borides, possesses a flexure strength in the range of 400-425 MPa, a fracture toughness of 5.8-6.2 MPa·m$^{1/2}$, a thermal conductivity of 70-96 W/m·K, a Vickers Hardness of 22-26 GPa, and good chemical stability.[1,2,3,5] These properties make TiB_2 attractive for applications such as cutting tools, wear resistant parts and armor materials.[1,4] Many toughening mechanisms have been used to extend the life of ceramics such as TiB_2 in tribological applications. Some methods include particulate, fiber, or whisker additions, as well as annealing.[5,6,7,8]

TiB_2 is difficult to densify without sintering additives and highly susceptible to microcracking during processing due to the large CTE mismatch between the major axes of its hexagonal crystal structure (6.6 x 10^{-6}/°C along the a-axis and 8.6 x 10^{-6}/°C along the c-axis)4. Silicon carbide (SiC) is a common additive to TiB_2, acting as a densification aid and limiting TiB_2 grain growth.[5,9,10] α-SiC has a CTE of 3.63 x 10^{-6}/°C along the a-axis and 4.16 x 10^{-6}/°C along the c-axis,[11] thus processing of TiB_2 - SiC ceramics results in residual thermal stresses leaving the TiB_2 phase in tension and the SiC in compression. TiB_2 – SiC particulate composites have been studied extensively, with several studies focused on increasing toughness via crack deflection caused by coarsened, elongated, TiB_2 grains.[5,6,12] While thermal stresses can have beneficial results, they can also cause microcracking. Altering the elastic properties and/or the CTE of one or both of the phases can reduce the magnitude of residual stress. Research on monolithic SiC has included methods of improving machinability of the material to reduce time and cost

while maintaining mechanical properties. Research incorporating 10 wt% BN in a SiC matrix resulted in ~30% reduction in elastic modulus with a 2-20% decrease in strength.[18,19]

The improvement of fracture toughness in ceramics is a major field of study within the ceramics community in order to better compete with metals. The task of creating a ceramic that exhibits graceful failure has followed a number of paths including, the addition of fibers, whiskers or producing engineered architectures such as fibrous monoliths. Fibrous monoliths consist of a hard, strong core material with a weaker interface or shell material. The shell allows the crack to deflect along the core while the core material maintains the load, fracturing individual or small quantities of cores at a time rather than the entire matrix. Zimmermann *et al.*[21] studied fibrous monoliths with ZrB_2-30 vol% SiC as the core and a graphite-ZrB_2 shell. The sample with 30 vol% ZrB_2 in the shell exhibited catastrophic failure but when ZrB_2 content is reduced to 15 vol% in the graphite shell graceful failure was observed. As a trade off with improving the fracture toughness, a decrease in strength is typically observed.

Previous research, using finite element modeling, indicated that altering the geometry of SiC additions in ZrB_2 may reduce the thermal residual stresses generated during cooling from the final sintering temperature[13]. The geometries of additions modeled were round, square, hexagonal, peanuts and spirals. The hexagonal geometry array resulted in increased residual stresses near corners of neighboring hexagonal SiC inclusions. However, this increase was not observed in the square array. The peanut geometry was created in light of the hexagonal and square geometry results to remove

sharp corners. The peanuts were oriented in an array in which the convex side of one was adjacent to the concave side of another, which resulted in a reduced stress field around the particles. In pursuit to model novel geometries, the spirals modeled resulted in a small decrease in the maximum tensile stresses, in comparison to that of the previous geometries; however, the difference between tensile and compressive stresses in the adjacent phases was decreased significantly. Preliminary research was performed to develop the processing techniques required to produce spiral shaped SiC inclusions as well as other shapes[13,14].

The production of the spiral architecture of SiC in TiB_2 matrix was the focus of this study with an evaluation of strength and fracture toughness. The nominal composition for this study was 75 vol.% TiB_2 - 25 vol.% SiC spirals, though variations in the composition were used to mitigate microcracking due to the CTE mismatch. A conventional TiB_2 sample reinforced with 25 vol.% SiC particles was used for comparison.

EXPERIMENTAL METHOD

TiB_2 powders (Grade HCT-F, Momentive Materials, Columbus, OH) and SiC powders (Grade UF-10, H.C. Starck, Goslar, Germany) were used as starting materials. Boron nitride (BN) powder (Grade HCP, Momentive Materials, Columbus, OH) was used as an additive in certain compositions. TiB_2 powders were ball milled with 2 wt% carbon (C) (Grade 120 Black Pearl, Cabot, Boston, MA) and 1 wt% boron carbide (B_4C) (Grade HD 20, H.C. Starck) in ethanol with TiB_2 media for 18 hours to ensure homogeneous

mixing of the sintering aids. The solvent was then removed via rotary evaporation and the powder was passed through a 60 mesh sieve.

Powders were blended with an ethylene ethyl acrylate (EEA) thermoplastic (Melt flow index = M.I. 1.5 or 20, Union Carbide, Danbury, CT) using a high shear mixer (C.W. Brabender, South Hackensack, NJ) at a temperature of 130°C. The milled TiB_2 powder was combined with EEA (M.I. 1.5) at ~56 vol.% solids loading, whereas as received SiC powder was combined with EEA (M.I. 20) at ~55 vol.% solids loading. Heavy mineral oil (Fisher Scientific, Fair Lawn, NJ) and polyethylene glycol methyl ether (Acros Organics, NJ) were used as plasticizers to adjust rheological properties. The individual polymer batches were then pressed into sheets with a nominal thickness of 1.3 mm using a heated hydraulic press (Model G50H-18-CX, Wabash MPI, Wabash, IN). The TiB_2 and SiC sheets were cut to nominally 22.8 x 7.6 cm and 7.6 x 7.6 cm rectangles, respectively, which results in the final respective 75 vol.% TiB_2 and 25 vol.% SiC composition. The size of each rectangle was adjusted accordingly based on the solids loading of the individual batches. The rectangular sheets could then be rolled into the spiral shape (illustrated in Figure 1) where the light gray layer is the SiC and the black layer is the TiB_2.

Figure 1. Schematic of the initial sheet layup which is then rolled up to the final spiral formation where the light gray is SiC and the black is TiB_2.

The cylindrical spiral was then pressed into a feedrod 22 mm in diameter by 7.6 cm long utilizing a hydraulic press and a heated die. The feedrod could then be extruded to a desired diameter for single filament co-extrusion (SFCX). The SFCX used in this study was extruded to a final diameter of 300 μm. For multi-filament co-extrusion (MFCX), filament from the SFCX, 2.4 mm in diameter unless otherwise noted, was cut to lengths similar to that of the original feedrod length (nominally ~6.5 cm) and gathered and pressed to form a secondary feedrod of multiple (~80) filaments. The secondary feedrod could then be extruded to a diameter of 1 mm for MFCX. The final filament was wound on a mandrel so that each filament lay next to, but not on top of, the other. The strips of laid-up filament were removed from the mandrel and chopped to lengths of 0.5 mm, 1.0 mm or 46 mm. The filament was chopped to 1 mm for the majority of the studies to produce a cube-like geometry and maximize the random orientation in the subsequent composites.

Table I lists the compositions along with the orientations of the spiral additions, the specimen IDs, the individual matrix and spiral compositions, spiral lengths, and the relative densities after hot pressing. The specimen IDs were determined to be the matrix component abbreviation before the dash and the spiral component abbreviation after the dash with the quantity of BN indicated. All MFCX spirals were extruded to a final diameter of 1 mm.

Table I. Details and Descriptions of Compositions

Composite	Specimen ID	Matrix Composition	Spiral Composition	Spiral Length (mm)	Relative Density (%)
Monolithic	M	TiB_2 + 25 vol% SiC	N/A	N/A	97.9
R.O. Spiral	T-S	TiB_2	SiC	1	97.6
R.O. Spiral	T-S10B	TiB_2	SiC + 10 wt% BN	1	93.5
R.O. Spiral	TS-S10B	TiB_2 + 5 vol% SiC	*SiC + 10 wt% BN	1	94.7
R.O. Spiral	TS-S	TiB_2 + 5 vol% SiC	*SiC	1	96.2
R.O. Spiral	T-S15B	TiB_2	SiC + 15 wt% BN	1	91.9
R.O. Spiral	T-S10B0.5	TiB_2	SiC + 10 wt% BN	0.5	90.4
0°	T-S10B46	TiB_2	SiC + 10 wt% BN	46	91.8

*20 vol% spiral additions

The green, chopped, spirals were poured into a 46 mm x 30 mm metal die and placed between heated platens at 130°C mounted on a uniaxial carver press (Model C, Fred S. Carver, Inc., Menomonee Falls, WI). The billet was pressed at 7 MPa for ~30 s at temperature. The billet was then transferred to a graphite hot press die (Graphite Products Corp., Madison Heights, MI) which was lined with grafoil and coated with boron nitride spray to limit interaction with the graphite die. The die was placed in a

controlled atmosphere retort furnace (Model 51542-HR, SPX: Thermal Product Solutions, Watertown, WI) for burnout of the polymer with a ramp rate of 20°C/hour to 600°C with a 2 hour hold, under an argon atmosphere. Once cool, the die was transferred to a graphite hot press (Model HP20-3060, Thermal Technologies, Santa Rosa, CA). The billets were heated at ~80°C/min under vacuum to 1650°C and held until vacuum pressure reached 200 mTorr (~1 hour). Following the hold at 1650°C the atmosphere was changed to argon, a pressure of 32 MPa was applied and the temperature was ramped to 1980°C at ~80°C/min. Ram travel of the hot press was monitored to determine densification. Specimens were held at temperature and pressure until ram travel had ceased for 10 minutes. The hot press was then cooled at ~50°C/min and pressure was released once the temperature reached 1650°C.

The powders for the TiB_2 – 25 vol.% SiC monolithic sample were ball milled together with 2 wt.% C and 1 wt.% B_4C in ethanol with TiB_2 media for 18 hrs to ensure thorough mixing. The ethanol was removed via rotary evaporation and powders were passed through a 60 mesh sieve. The die preparation and hot pressing schedule was identical to that of the spiral samples, except that the burnout procedure was omitted.

Billets were machined into mechanical test bars using an automated surface grinder (Model FSG-3A818, Chevalier Machinery Inc., Santa Fe Springs, CA). Flexure bars were machined following ASTM C1161-02c for B-bars (3 mm x 4 mm x 45 mm) and chevron notch bars were prepared according to ASTM C1421-10 for A-bars (4 mm x 3 mm x 45 mm) with a 600 grit final surface finish. In addition, the tensile surface of the flexure bars was polished to a 0.25 μm finish using successively finer diamond slurries.

Specimens were tested in four point bending with a fully articulated fixture (40 mm lower span and 20 mm upper span) using a screw-driven load frame (Model 5881, Instron, Norwood, MA) controlled by Bluehill 2 software. Fracture toughness was measured using chevron notch modified A-bars. The A-bars were modified to be ~22 mm in length and tested using a semi- articulated fixture (20 mm support span, 10 mm upper span). The load rate was adjusted to remain within the standard strain rate (0.00045 s^{-1}) specified by the standard.

Density of the specimens was measured using Archimedes method. Theoretical densities of 4.19, 4.15 and 4.13 g/cm^3 for $TiB_2 - 25$ vol.% SiC, $TiB_2 - 25$ vol.% SiC with 10 and 15 wt% BN, respectively, was used. These densities were calculated using a volumetric rule of mixtures using densities of 4.52, 3.21, and 2.10 g/cm^3 for TiB_2, SiC and BN, respectively.

Vickers indents (Duramin 5, Struers Inc., Cleveland, OH), using a load of 9.8 N (1 kg) with a 10 s dwell time, were used to observe the crack deflection caused by the spiral additions.

Specimens were polished to a 0.25 µm finish using successively finer diamond slurries to be examined using optical microscopy (Epiphot 200, Nikon, Tokyo, Japan) as well as scanning electron microscopy (S-570 Hitachi, Tokyo, Japan). Microscopy was conducted to view the morphology of the sintered spirals, look for micro/macro-cracking, and observe crack paths.

RESULTS & DISCUSSION

Hot pressed M and T-S samples reached near full density (>96%) including the MFCX experiments conducted to determine the parameters for the most desirable outcome of microstructure with respect to the spiral geometry (Figure 2). Figure 3 illustrates the resulting microstructure of the SFCX composites. The smallest SFCX filaments, 300 μm diameter, resulted in a spiral approximately 180 μm in diameter and the lowest density of the T-S compositions of 93%. With optical microscopy, large porosity and cracking were observed (Figure 3). The compositions with BN additions resulted in lower relative densities, 90-95%, which can be observed in Figure 4. In all the MFCX compositions microcracking was observed throughout the TiB_2 matrix as well as within the TiB_2 spiral layers, as shown in Figure 5 and Figure 6, though to varying degrees with each of the compositions.

To mitigate the microcracking, the spiral sizes were reduced by moving to MFCX. MFCX with an initial extrusion to 4 mm and final extrusion to 1mm (4 mm/1 mm) resulted in a spiral diameter of ~120 um, similar to that of the 300 μm SFCX. Therefore, reduction of the initial co-extrusion diameter was considered, keeping the final MFCX diameter constant. The initial SFCX diameter of 2.4 mm resulted in consistent spiral geometries throughout with a diameter of approximately 50 μm. However, the 1.75 mm/1 mm SFCX did not produce a consistent architecture. The calculated spiral layers from the 1.75 mm/1 mm and 1 mm/1 mm MFCX were 5 μm and 3 μm thick, respectively, which is on the same order as the particle size of the starting powders.

Thus, the ultimate size of the MFCX spiral architecture was limited by the particle size of

the TiB$_2$.

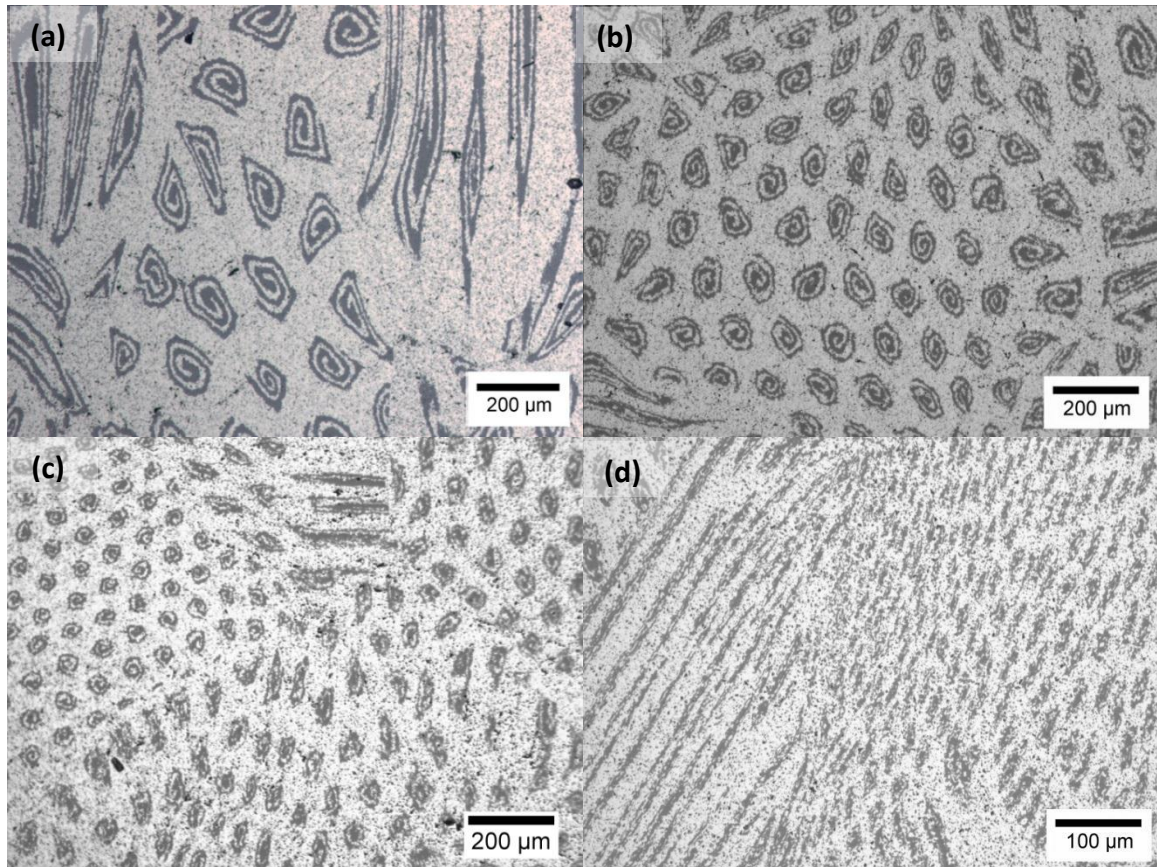Figure 2. Optical images of MFCX experiments 4mm/1mm (a), 2.4mm/1mm (b), 1.75mm/1mm (c), 1mm/1mm (d).
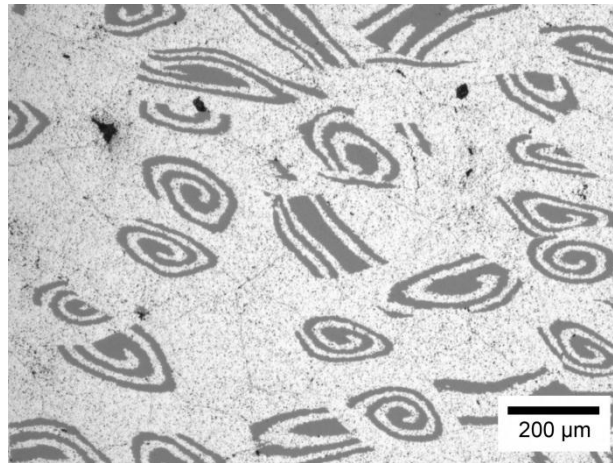
Figure 3. Optical image of 300 µm SFCX indicates significant amounts of microcracking with spirals ~180 um in diameter.
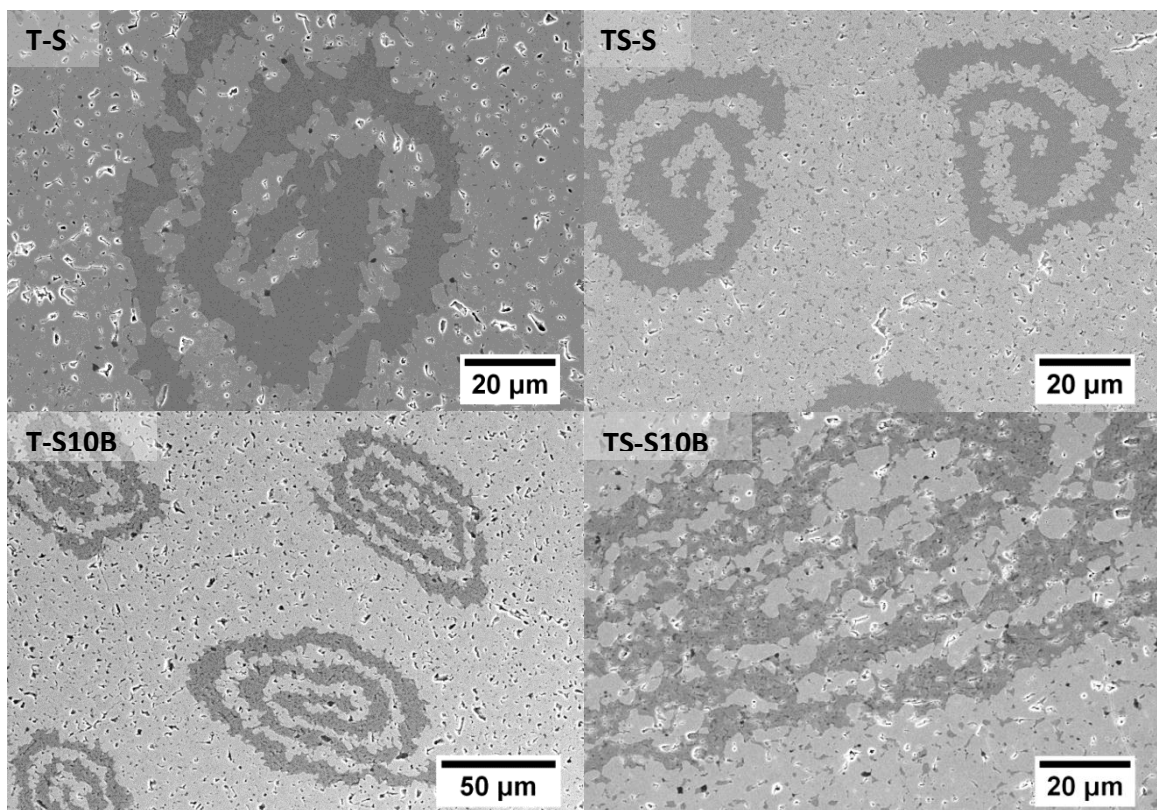
Figure 4. SEM images of T-S, TS-S, T-S10B and TS-S10B specimens show the nominal microstructure of the specimens. The light gray is TiB_2, dark gray is SiC and black phase is residual C.

Within the 2.4 mm/1 mm MFCX microcracking could be observed throughout the matrix, as well as within, and around the spirals. Ultimately, spirals were not able to be produced small enough to eliminate cracking due to the CTE mismatch between the TiB$_2$ and SiC. Thermal stresses generated from processing can be estimated using Equation 1.[15]

$$\sigma_{tan} = -\frac{P}{1-V_p}\left[\frac{1}{2}\frac{a^3}{r^3} + V_p\right] \tag{1}$$

This discribes for the tangential stress, σ_{tan}, at the surface of a particle where P is the stress within the particle, a is the radius of the particle, r is the distance from the center of the particle and V_p is the volume fraction of particles. For the tangential stress at the surface of a particle, a=r. For TiB$_2$-25 vol% SiC the tangential stress created is ~4 GPa, considerably higher than that of a stress which either monolithic material is able to withstand. Previous research indicates a TiB$_2$ grain size >15 μm results in spontaneous microcracking in the TiB$_2$ matrix due to TiB$_2$'s CTE mismatch and the resulting residual stresses. [2,16,17]

Up to this point no additives other than the sintering aids were employed. In a further attempt to mitigate the microcracking, additives were used to alter the elastic properties as well as the CTE mismatch between phases. SiC was added in particulate form to the TiB$_2$ matrix and BN was added to the SiC spirals. BN has been used in studies to improve machinability and thermal shock resistance of SiC with minimal effect on strength while decreasing the elastic modulus.[18,19] The microstructures in Figure 4 illustrate the nominal microstructure of the different compositions. The density decreased with the addition of BN in the spiral with a noticeable presence of pore

coalescence in the TS-S specimen. Visually there was no apparent reduction in microcracking. Though not evident in Figure 4, Figure 6 illustrates the microcracking observed in between the spiral layers of the T-S specimen, specifically, which was observed in all other specimens as well.
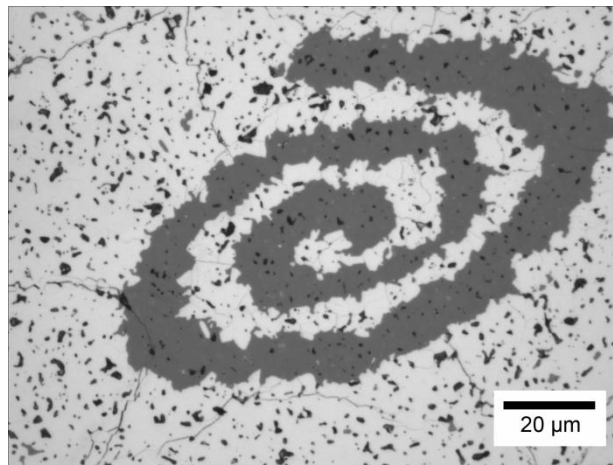
Figure 5. Spiral from 4 mm/1 mm MFCX surrounded by microcracking in the TiB$_2$ matrix
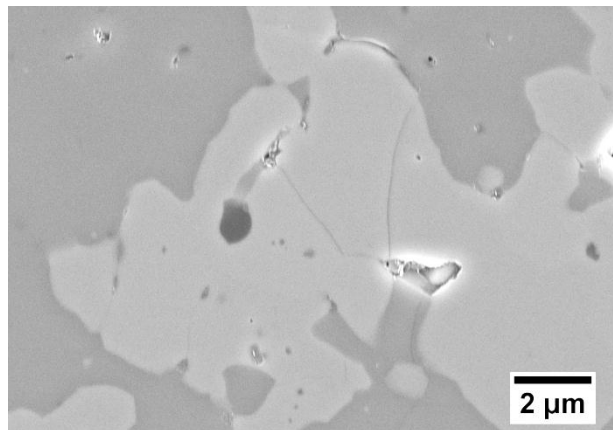
Figure 6. Example of microcracking between spiral layers in T-S specimen.

The mechanical testing results are summarized in Table II. The monolithic specimens resulted in an average fracture strength of 488 ± 45 MPa and fracture toughness of 5.3 ± 0.4 MPa·m$^{1/2}$. The maximum strength of the spiral samples was measured from the T-S10B specimen at 222 ± 20 MPa, which is below 50% of the monolithic in strength. However, with respect to other co-extruded architectures, fibrous monoliths, a significant decrease in strength is common, such as a 55% reduction for ZrB_2 – 30vol% SiC with a graphite-based cell boundary phase in comparison to a simple particulate addition[20,21]. In comparison, an approximate 30% reduction with the addition of fibers such as TiB_2 with 5 wt.% carbon fiber[8] or SiC chopped fibers in a ZrB_2 matrix.[22,23].

Table II. Spiral Mechanical Properties

Specimen ID	Relative Density	Fracture Strength (MPa)			Fracture Toughness (MPa·m$^{1/2}$)		
M	97.9%	488	±	45	5.3	±	0.4
T-S	97.6%	212	±	7	8.2	±	0.0
T-S10B	93.5%	222	±	20	7.0	±	0.8
TS-S10B	94.7%	146	±	35	7.7	±	0.8
TS-S	96.2%	201	±	7	8.0	±	0.8
T-S15B	91.9%	214	±	16	6.8	±	0.9
T-S10B0.5	90.4%	185	±	39	7.3	±	0.4
T-S10B46	91.8%	200	±	2	7.5	±	0.4

The reduction of strength is a tradeoff for the added fracture toughness. The addition of spirals led to an average 40% increase in fracture toughness. When measuring fracture toughness, the direct crack method could not be used due to substantial crack deflection in and around the spirals, as can be observed in Figure 7.

The indent placed in the TiB_2 matrix (a) is in a region where there are multiple spirals with the same orientation. The radial-median cracks from the indent follow the same orientation as the spirals instead of extending straight out from the corners of the Vickers indent. The indent, seen in image b, within the SiC spiral shows that the radial cracks are deflected along the SiC – TiB_2 boundary layers, never escaping the final spiral layer and returning to the matrix.
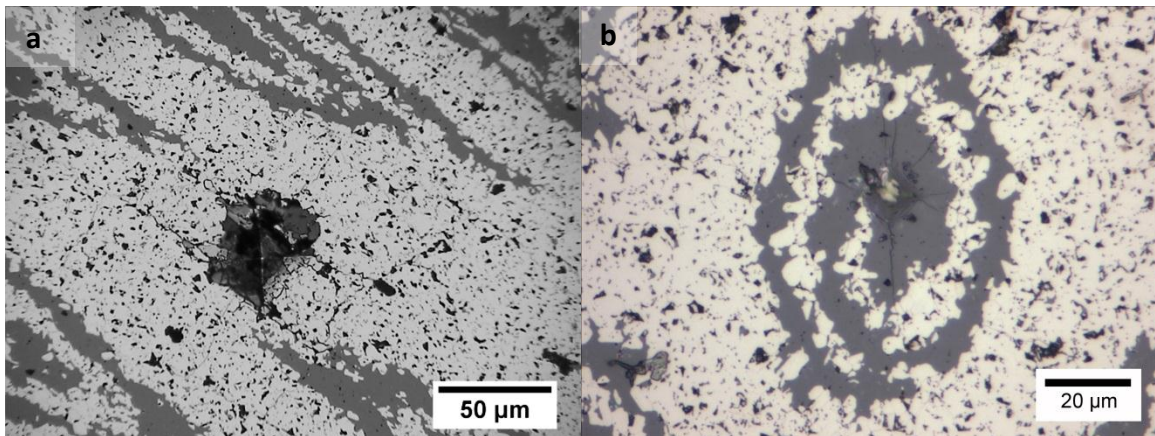
Figure 7. Vickers indent in TiB2 matrix (a) as well as within SiC spiral (b) indicates significant crack deflection.

In order to determine trends in the specimens tested, the results were analyzed as three related categories; increasing BN content, increasing additives, and increasing spiral length. With increasing BN content of 0 wt%, 10 wt% and 15 wt% within the SiC spiral layer, illustrated in Figure 8, there is a slight decrease in fracture toughness, from ~8.2 to 6.8 MPa·m$^{1/2}$, but not a significant difference in strength (212 MPa to 222 MPa).

As the additive content increased from none to 5 vol.% SiC in the TiB_2 matrix, with as 10 wt% BN in the SiC spirals, the fracture toughness remained relatively

unchanged, from 8.2 to 7.7 MPa·m$^{1/2}$, with strength showing a significant decrease,

from ~212 MPa to 146 MPa, as illustrated in Figure 9.

In an effort to determine the dominating critical flaw size, the study continued

with a variation of spiral length from the nominal 1 mm to 0.5 mm and a 46 mm, 0°

uniaxial layup. The T-S10B composition was chosen to continue the study due to the

similar or superior mechanical properties compared to other compositions in the study

and the visual evaluation of the microstructures. There was not a significant change in

fracture toughness as the spiral length changed 7.0-7.5 MPa·m$^{1/2}$, as illustrated in Figure

10. Though the magnitude of the strength did not vary considerably, 185-222 MPa, the

standard deviation of the strength narrowed from ± 39 MPa for the 0.5 mm spiral

lengths to ± 2 MPa for the uniaxial specimen. As the spiral length changed, there was no

noticeable difference in fracture toughness, though the opposite would have been

thought true if the spiral length were related to the critical flaw size.

The critical flaw size was calculated using the Griffith criteria (Equation 1)[24]

$$c = \left(\frac{K_{IC}}{\sigma_f Y}\right)^2 \qquad (1)$$

Where c is the critical flaw size, K_{IC} is the fracture toughness, σ_f is the failure

strength, and Y is the crack geometry constant for an internal circular or penny crack

found in Equation 2.[24]

$$Y = \frac{2}{\sqrt{\pi}} \qquad (2)$$

The calculated critical flaw sizes were around the 1 mm range, which is about the

same as the spiral length for most of the samples. However, the 0.5 mm and the 46 mm

specimens, also resulted in critical flaw sizes of approximately 1 mm, which indicates the critical flaw size may correlate with the filament diameter rather than the spiral length.

While matrix cracking was reduced, it was still present in all the specimens tested. Thus, concluding the critical flaw size is related to the filament diameter is difficult. Future work with a change in composition will be considered to determine the acting flaw size in the MFCX materials.
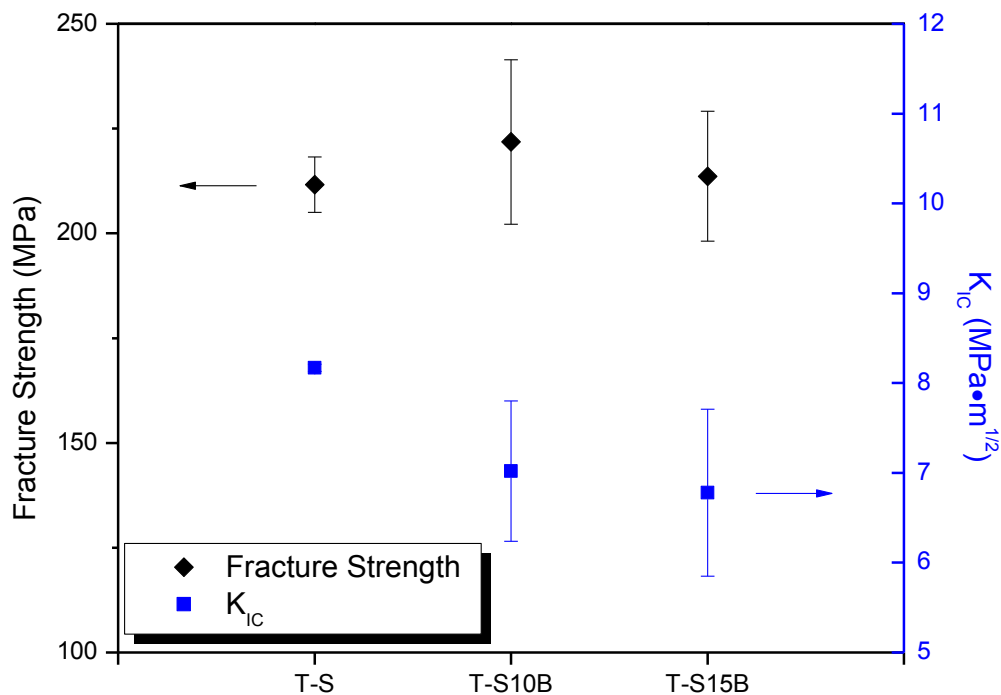
Figure 8. Fracture strength and toughness of specimens with increasing BN content from 0 wt%, 10 wt% and 15 wt% within the SiC spiral layer.
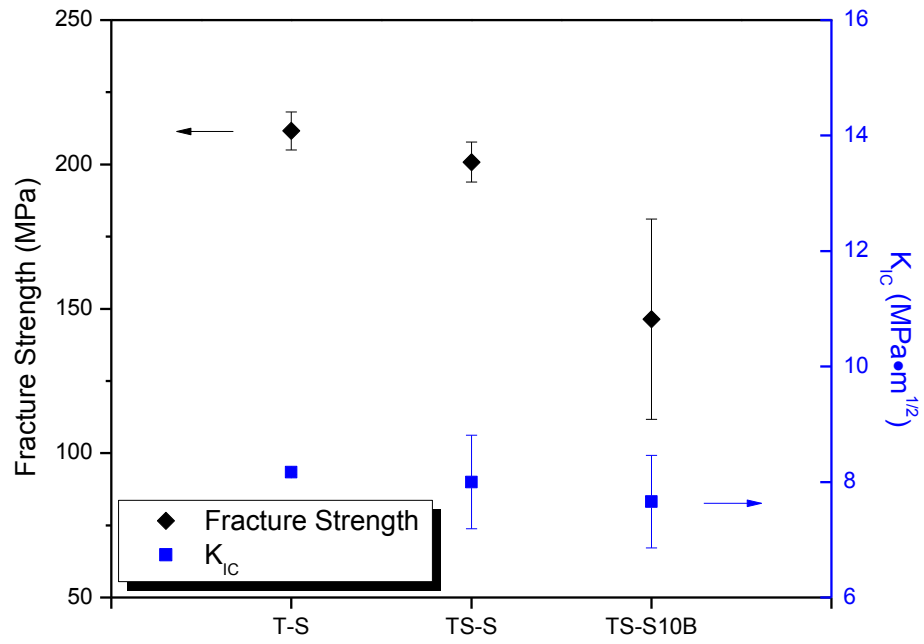
Figure 9. Fracture strength and toughness of specimens with increasing additives from the base TiB$_2$-SiC to 5 vol% SiC in the TiB$_2$ matrix and finaly both 5 vol% SiC in the TiB$_2$ matrix as well as 10 wt% BN in the SiC spiral layer
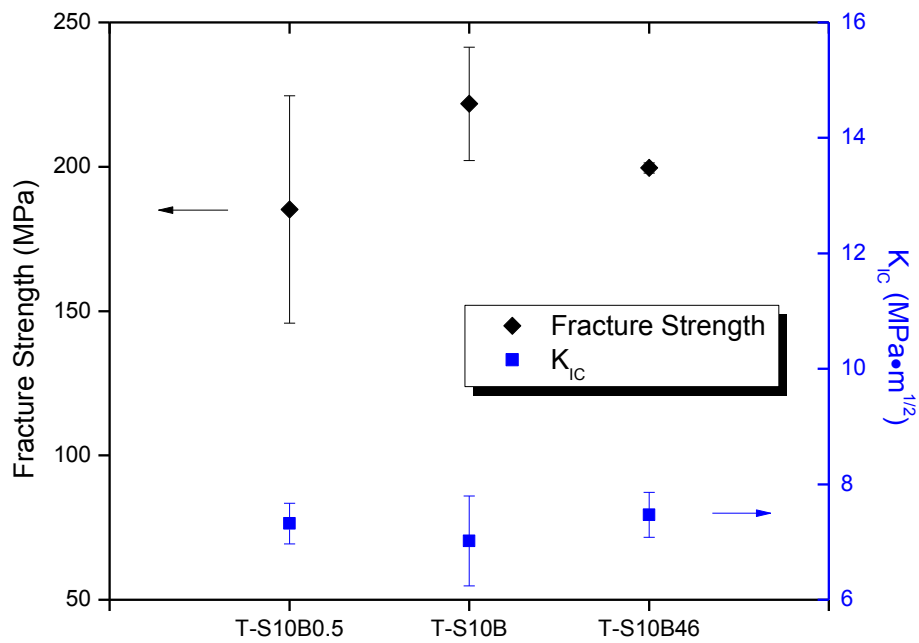
Figure 10. Fracture strength and toughness of constant composition and increasing spiral length of 0.5 mm, 1 mm, and 46mm spirals.
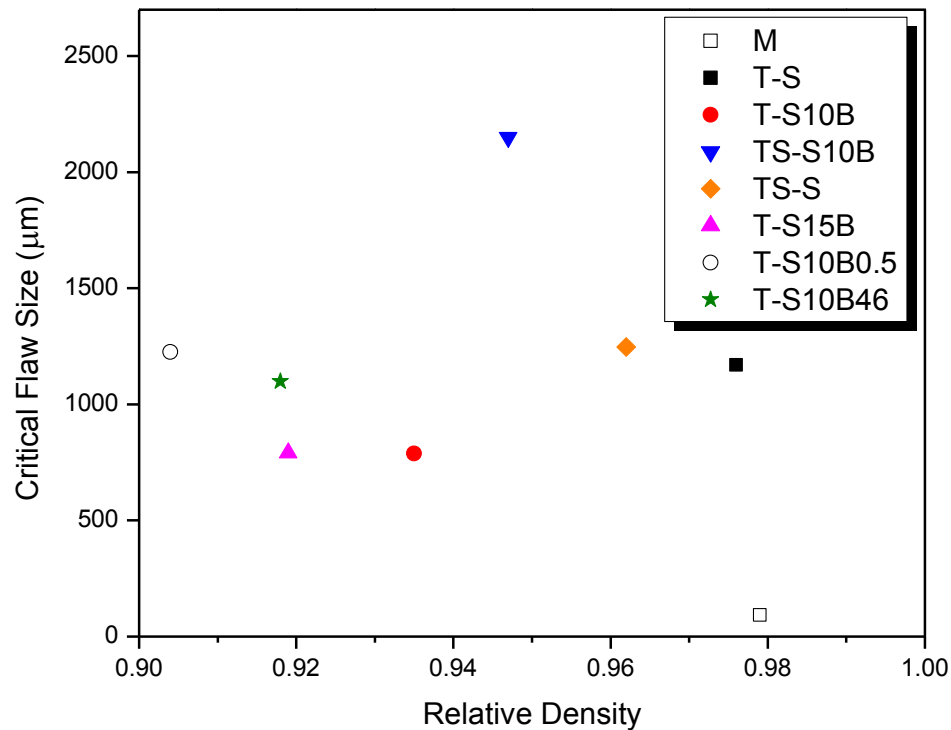
Figure 11. Calculated critical flaw size with respect to density is unrelated, though the critical flaw size for the majority of the specimens is ~1000 μm.

CONCLUSIONS

Co-extrusion was used to develop a spiral architecture to improve the fracture toughness of TiB$_2$-25 vol% SiC ceramics. The spiral size was minimized to ~50 μm in diameter, at which point the particle size of the constituent powders became the limiting factor. The additions of the spirals decreased the fracture strength ~60% on average with an average strength of 193 MPa in comparison to the 488 MPa exhibited by the monolithic material. However, a fracture toughness boost was achieved of ~40% on average, exhibiting a peak fracture toughness of 8.2 MPa·m$^{1/2}$ (an increase of 55%).

Various compositions were used in attempts to mitigate microcracking. While cracking

was reduced, it was not eliminated. The critical flaw size correlates well with the

filament diameter, though the microcracking throughout the matrix must be resolved

before this can be determined conclusively. A major alteration in bulk composition will

be investigated in the future.

ACKNOWLEDGEMENTS

REFERENCES

1. R. A. Cutler, "Engineering Properties of Borides," pp. 787-803. in *Ceramics and Glasses, Engineered Materials Handbook,* **Vol. 4.** Edited by S. J. Schneider Jr. ASM International, Materials Park, OH, 1991.

2. Ferber MK, Becher PF, Finch CB. Effect of microstructure on the properties of TiB2 ceramics. *J Am Ceram Soc* 1983;**66**(1):C-2–3.

3. Munro RG. Material properties of titanium diboride. *Journal of Research of the National Institute of Standards and Technology*. 2000;105(5):709-20

4. Basu B, Processing and properties of monolithic TiB2 based materials. *Int Mater Rev* 2006; **51**(6):352-74

5. King DS, Fahrenholtz WG, Hilmas GE. Silicon carbide-titanium diboride ceramic composites. *J Am Ceram Soc*. 2013;33(15-16):2943-51

6. Cho K, Choi H, Lee J, Kim Y. In situ enhancement of toughness of SiC-TiB2 composites. *J Mat'l Sci*. 1998;33(1):211-4.

7. Kamiya A, Nakano K, Kondoh A, "Fabrication and properties of hot-pressed SiC whisker-reinforced TiB2 and TiC composites." *J. of Mat'l. Sci*. Letters **8** 566-568 (1989)

8. Fei J, Wang W, Ren A, Ji Y, Zhou J, Zhu M. Mechanical properties and densification of short carbon fiber-reinforced TiB2/C composites produced by hot pressing. *Journal of Alloys and Compounds*. **584**. 87-92 (2014)

9. Chen Y, Jiang L, Jia X. Properties of pressureless sintered SiC-TiB2 composites. 2010, Advanced Materials Research, 177, 369

10. Ran S, Zhang L, Van der Biest O, Vleugels J,. Pulsed electric current, in situ synthesis and sintering of textured TiB2 ceramics. *Journal of the European Ceramic Society, 30*(4), 1043-1047. (2010)

11. Li Z, Bradt RC. Thermal expansion and thermal expansion anisotropy of SiC polytypes. *J Am Ceram Soc* 1987;**70**(7):445–8

12. Zhao G, Huang C, Liu H, Zou B, Zhu H, Wang J, "Microstructure and mechanical properties of TiB2-SiC ceramic composites by Reactive Hot Pressing" Int. Journal of Refractory Metals and Hard Materials" 42 (2014) 36-41

13. Teague M, "Modeing and Measurement of Thermal Residual Stresses and Isotope Effects on Thermo Physical Properties of ZrB2-SiC Ceramics," Materials Sience and Engineering, Missouri University of Science and Technology, Master of Science, 2008

14. Watts J, Hilmas G, Fahrenholtz W, "A Method for Toughening via the Production of Spiral Architectures Through Powder Loaded Polymer Extrusion and Toughened Materials Formed Thereby," United States Patent, 8,192,853, 2012

15. Cawla K, Composite Materials Science and Engineering, Second Edition. Springer-Verlag, New York, 1998. 332-3

16. Tennery V, Finch C, Yust C, Clark G," Structure-Property Correlations for TiB2-based Ceramics Densified Using Active Liquid Metals" Science of Hard Materials. Plenum, New York, 1981. 891-901

17. Bamgartner H, Steiger R, "Sintering and Properties of Titanium Diboride Made from Powder Synthesized in a Plasma-Arc Heater", *J. Am. Ceram. Soc*. **67** (1984) 207-12

18. Jin H, Qiao G, Gao J, "Investigation of Thermal Shock Behaviors for Machinable SiC/h-BN Ceramic Composites." Material Science Forum, [544-545] 391-394 (2007)

19. X. Wang, G. Qiao, Z. Jin, "Fabrication of Machinable Silicon Carbide-Boron Nitride Ceramic Nanocomposites." *J. Am. Ceram. Soc*., 87 [4] 565-70 (2004)

20. Fahrenholtz WG, Hilmas GE, Chamberlain AL, Zimmermann JW, Processing and characterization of ZrB2 – based ultra-high temperature monolithic and fibrous monolithic ceramics. *J Mat'l Sci*. 39 [19] 5951-5957 (2004)

21. Zimmermann JW, Hilmas GE, Fahrenholtz WG, Thermal Shock Resistance and Fracture Behavior of ZrB2–Based Fibrous Monolith Ceramics. *J Am Ceram Soc.* 92 [1] 161-166 (2009)

22.   Guicciardi S, Silvestroni L, Nygren M, Sciti D. Microstructure and toughening mechanisms in spark plasma-sintered ZrB2 ceramics reinforced by SiC whiskers or SiC-chopped fibers. *J Am Ceram Soc*. 2010;93(8):2384-91

23.   Silvestroni L, Sciti D, Melandri C, Guicciardi S, Toughened ZrB2-based ceramics through SiC whisker or SiC chopped fiber additions, Journal of the European Ceramic Society, 30, [11], August 2010, Pages 2155-2164

24.   Green DJ, An Introduction to the Mechanical Properties of Ceramics. 1998. Cambridge University Press. 222-6

II. PROCESSING AND PROPERTIES OF SIC-TIB$_2$ CERAMICS CONTAINING A SPIRAL ARCHITECTURE

Andrea Els, Jeremy Watts, Greg Hilmas, William Fahrenholtz

ABSTRACT

Titanium diboride spirals were incorporated into a silicon carbide matrix at a nominal 25 vol.%. Powder loaded thermoplastic was used to create the geometries, followed by single and/or multi-filament co-extrusion. Varying spiral lengths and diameters were studied in order to determine critical flaw size of the composites with spiral additions and compared with that of a monolithic SiC-TiB$_2$ composition. All samples were hot pressed to near full density at 1980°C. Room temperature flexure strength of the monolithic composition was 418 ± 41 MPa with the spiral compositions averaging 313 ± 11 MPa. The fracture toughness of 3.8 ± 0.6 MPa·m$^{1/2}$ for the monolithic was increased to 6.2 ± 0.4 MPa·m$^{1/2}$ with the addition of spirals. The boost in fracture toughness is due to increased crack deflection in and around the TiB$_2$ spiral inclusions. Wear testing of the monolithic and uniaxial spiral specimens resulted in 1.1 mm^3 and 3.3 mm^3 of wear per 6,000 revolutions, respectively, with preferential wear of the uniaxial spiral sections. Post-wear flexure tests resulted in a 16% increase in the flexure strength of the uniaxial spiral architectures, whereas the monolithic exhibited an 18% decrease.

INTRODUCTION

Silicon carbide (SiC) is strong (305-412 MPa), hard (20-27 GPa), thermally conductive (105-123 W m^{-1} K^{-1}), and chemically inert [1,2,3]. These properties make it ideal for high temperature applications as well as structural, armor, and electrical. However, it has a low fracture toughness which makes it especially difficult to implement in structural applications due to catastrophic failure. Through incorporation of expensive fibers and 3D fiber braids, however, some researchers have cited K_{IC} values as high as 29.7 MPa·m$^{1/2}$.[4] Many armor researchers have investigated particulate titanium diboride (TiB$_2$) additions due to its desirable properties in the similar categories as SiC which makes it a compatible additive. They have shown with the addition of TiB$_2$ to SiC fracture toughness is improved due to increased crack deflection.[5,6]

The improvement of fracture toughness in ceramics is a major field of study within the ceramics community. The task of creating a ceramic that exhibits graceful failure has been attempted through a variety of methods, including, the addition of fibers, whiskers, particulates or engineered architectures such as fibrous monoliths. Fibrous monoliths consist of a hard, strong core material with a weaker interface or shell material. The shell allows the crack to deflect along the core while the core material maintains the load, fracturing individual or small quantities of cores at a time rather than the entire matrix. By altering the microstructure to improve fracture toughness however, comes at the expense of decreased strength. [6,7,8]

In many cases, forming a composite with multiple phases results in the generation of thermal residual stresses due to the variation in coefficients of thermal

expansion (CTE) between materials. These residual stresses can be beneficial, however if they are too large, micro or even macro cracking can develop.[9,10] Previous studies with finite element modeling suggest that altering the geometry of SiC additions to a spiral shape in a zirconium diboride matrix may reduce the difference in thermal residual stresses[11]. Co-extrusion has been used to form SiC spiral geometries successfully in the as modeled ZrB_2 matrix[12] as well as in a TiB_2 matrix[13]. However, in both of those studies the residual thermal stresses were such that spontaneous microcracking occurred in the matrix phase.

The current study focuses on the production of a spiral architecture consisting of TiB_2 spirals in a SiC matrix. A nominal composition of 25 vol.% TiB_2 spirals in SiC matrix was used along with a particulate composite of the same overall composition for comparison. Unlike the previous studies[13], the material with the higher CTE will be used as the spiral phase which should reverse the CTE mismatch and eliminate the matrix cracking.

EXPERIMENTAL METHOD

SiC powder (Grade UF-10, H.C. Starck, Goslar, Germany) and TiB_2 powder (Grade HCT-F, Momentive Materials, Columbus, OH) were used for the starting compositions. SiC and TiB_2 powders were ball milled separately, each with 2 wt% carbon (C) (Grade 120 Black Pearl, Cabot, Boston, MA) and 1 wt% boron carbide (B_4C) (Grade HD 20, H.C. Starck) in ethanol with TiB_2 media for 18 hours to ensure homogeneous mixing of the sintering aids. The solvent was then removed via rotary evaporation and the powder was passed through a 60 mesh sieve.

Powders were blended with an ethylene ethyl acrylate (EEA) thermoplastic (Melt flow index = M.I. 1.5 or 20, Union Carbide, Danbury, CT), using a high shear mixer (C.W. Brabender, South Hackensack, NJ) at a temperature of 130°C. The milled SiC powder was combined with EEA (M.I. 20) at ~55 vol.% solids loading, whereas TiB_2 powder was combined with EEA (M.I. 1.5) at ~56 vol.% solids loading. Heavy mineral oil (HMO) (Fisher Scientific, Fair Lawn, NJ) and polyethylene glycol methyl ether (MPEG) (Acros Organics, NJ) were used as plasticizers to adjust rheological properties. The individual polymer batches were then pressed into sheets with a nominal thickness of 1.3 mm using a heated hydraulic press (Wabash MPI, Model G50H-18-CX, Wabash, IN). The SiC and TiB_2 sheets were cut to nominally 22.8 x 7.6 cm and 7.6 x 7.6 cm rectangles, respectively, which results in the final respective 75 vol.% SiC and 25 vol.% TiB_2 composition. The size of each rectangle was adjusted accordingly based on the solids loading of the individual batches. The rectangular sheets could then be rolled into the spiral shape illustrated in Figure 1 where the light gray is the SiC and the black layer is the TiB_2.

Figure 1. Schematic of the initial sheet layup which is then rolled up to the final spiral formation where the light gray is SiC and the black is TiB_2

The cylindrical spiral was then pressed into a feedrod 22 mm in diameter by 7.6 cm long utilizing a hydraulic press and a heated die. The feedrod was extruded to a diameter of 300 µm for single filament co-extrusion (SFCX). For multi-filament co-extrusion (MFCX), filament was initially extruded to a diameter of 2.4 mm. The filament was then cut to lengths similar to that of the original feedrod length (~6.5 cm) and gathered and pressed to form a secondary feedrod of multiple filaments. The secondary feedrod was then extruded to a diameter of 1 mm (MFCX). The final filament was wound on a mandrel so that each filament lay next to, but not on top of, the other. The strips of laid-up filament were removed from the mandrel and chopped to 300 µm for the SFCX and 0.5 mm, 1.0 mm or 46 mm for the MFCX. Details of the compositions studied are listed in Table I.

Table I. Description and Details of Compositions Studied.

Composite	Specimen ID	Matrix Composition	Spiral Composition	Spiral Length	Relative Density
Monolithic	SM	SiC + 25 vol% TiB_2	N/A	N/A	98.0
R.O. Spiral	S-T300	SiC	TiB_2	300 µm	97.1
R.O. Spiral	S-T0.5	SiC	TiB_2	0.5 mm	97.7
R.O. Spiral	S-T1	SiC	TiB_2	1 mm	97.2
0°	S-T46	SiC	TiB_2	46 mm	98.0

The green, chopped, spirals were poured into a 46 mm x 30 mm metal die and placed between heated platens at 130°C mounted on a uniaxial press (Fred S Carver,

Inc., Model C, Menomonee Falls, WI). The billet was pressed at 7 MPa for ~30 s at temperature. The billet was transferred to a graphite hot press die (Graphite Products Corp., Madison Heights, MI) which was lined with grafoil and coated with boron nitride spray to limit interaction with the graphite die. The die was placed in a furnace atmosphere retort (SPX: Thermal Product Solutions, Model 51542-HR, Watertown, WI) for burnout of the polymer with a ramp rate of 20°C/hour to 600°C with a 2 hour hold all under an argon atmosphere. Once cool, the die was transferred to a graphite hot press (Thermal Technologies, Model HP20-3060, Santa Rosa, CA). Specimens were heated at ~80°C/min under vacuum to 1650°C and held until vacuum pressure reached 200 mTorr (~1 hour). Following the hold at 1650°C the atmosphere was changed to argon, a pressure of 32 MPa was applied and the temperature was ramped to 1980°C at ~80°C/min. Ram travel of the hot press was monitored to determine densification. Specimens were held at temperature and pressure until ram travel had ceased for 10 minutes. The hot press was then cooled at ~50°C/min and pressure was released once the temperature reached 1650°C.

Billets were machined into mechanical test bars using an automated surface grinder (Chevalier Machinery Inc., Model FSG-3A818, Santa Fe Springs, CA). Flexure bars were machined following ASTM C1161-02c[14] for B-bars (3 mm x 4 mm x 45 mm) and chevron notch bars were prepared according to ASTM C1421-10 for A-bars (4 mm x 3 mm x 45 mm) with a 600 grit final surface finish. In addition, the tensile surface for flexure B-bars was polished to a 0.25 μm finish using successively finer diamond slurries. Specimens were tested in four point bending with a fully articulated fixture (40 mm

support span and 20 mm load span) using a screw-driven load frame (Instron, Model

5881, Norwood, MA) controlled by Bluehill 2 software. Fracture toughness was

measured using chevron notch modified A-bars for the spiral compositions. The A-bars

were modified to be ~22 mm in length and tested using a semi- articulating fixture (20

mm support span and 10 mm load span). The load rate was adjusted to remain

maintain a strain rate in the range specified in the standard. For the monolithic

specimen, chevron notch tests produced invalid load-deflection curves; therefore,

fracture toughness was measured using direct crack measurements. Indents (Leco

Corporation, Model V-100-A2, St. Joseph, MI) were made using a 49 N (5 kg) load for 15

s with a diamond Vickers indenter.

Vickers indents (Struers Inc., Duramin 5, Cleveland, OH) using a load of 19.6 N (2

kg) with a 10 s dwell time were used to observe the crack deflection caused by the spiral

additions.

Wear testing was done according to ASTM G65.[15] The faces of the hot pressed

billets were ground parallel with a 600 grit diamond wheel. For post-wear flexure tests,

the billets were cut so that two flexure B-bars could be made from the wear scar as well

as three bars from the unworn portion of the same billet. The three sides of the bar that

were not on the wear surface were ground to meet the B-bar specimen size indicated in

ASTM C1161.[14] The worn specimens were oriented such that the wear scar in tension

spanned the entire 20 mm load span.

Specimens for microscopy were prepared by polishing to a 0.25 μm finish

utilizing diamond pads or diamond slurries in decreasing increments. The specimens

could then be examined using optical microscopy (Epiphot 200, Nikon, Tokyo, Japan) as well as scanning electron microscopy (S-570 Hitachi, Tokyo, Japan).

RESULTS & DISCUSSION

All the samples reached greater than 97% of their theoretical density via hot pressing. Similar to previous studies with spiral architectures[12,13], microcracking can be observed in the uniaxial sample (S-T46) in Figure 2, pointed out by the arrows. However, unlike those previous studies, the microcracking is confined to the spiral phase instead of the matrix material. This was expected due to the CTE mismatch between the TiB_2 and SiC. The SFCX to 300 μm (S-T300) resulted in a spiral diameter of ~180 μm, whereas the MFCX of 2.4 mm/1 mm resulted in a spiral diameter of ~50 μm.
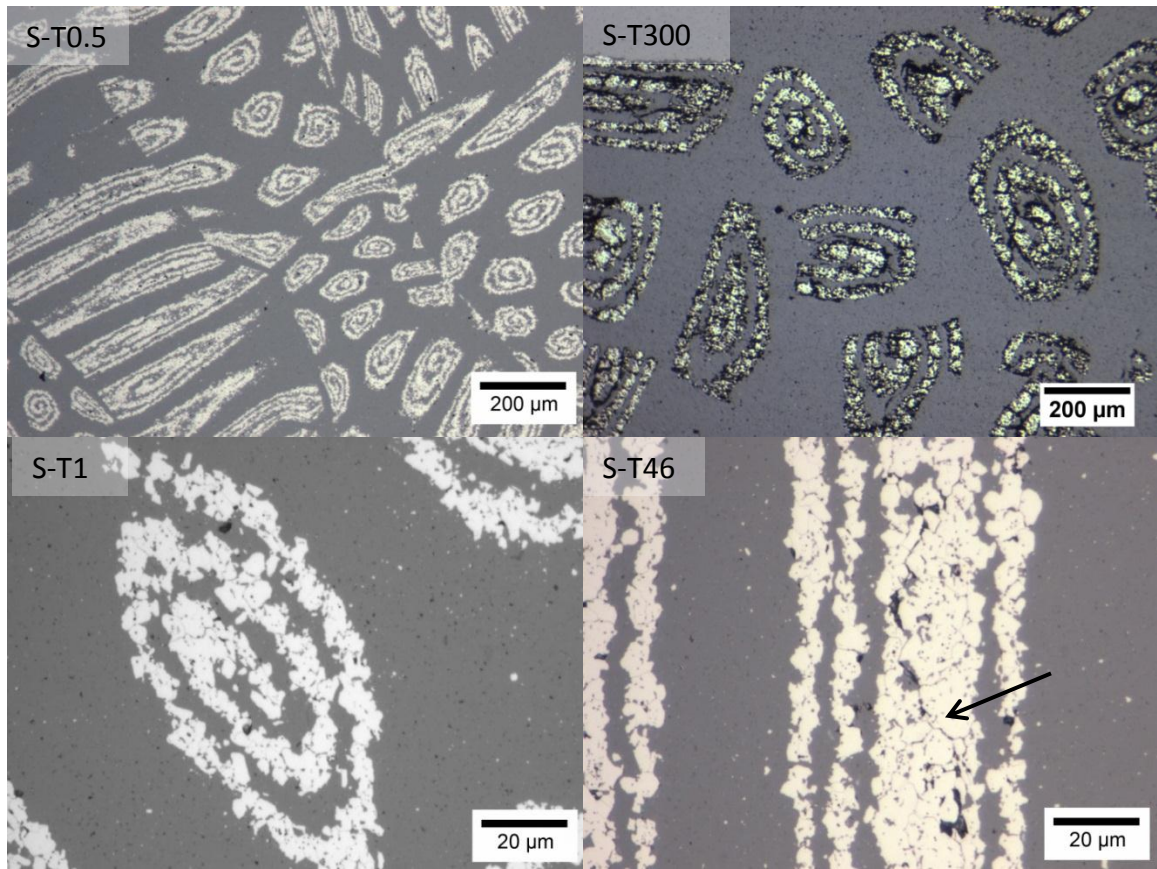
Figure 2. Optical images at various magnifications of MFCX specimen lengths of 0.5 mm (S-T0.5), 1 mm (S-T1) and 46 mm (S-T46) and SFCX specimen with spiral length of 300 µm (S-T300).

With respect to mechanical testing, results of which are detailed in Table II and Figure 3, the conventional particulate composite resulted in an average fracture strength of 418 ± 41 MPa and a fracture toughness of 3.8 ± 0.6 MPa·m$^{1/2}$. The strength of the spiral samples increased with increasing spiral length, with the maximum strength exhibited by the uniaxial sample at 294 ± 21 MPa. On average, the spiral additions had approximately 46% lower strength than that of the monolithic, 224 ± 51 MPa. Fracture toughness also increased with increasing spiral length up to the 1 mm specimen with a

K_{IC} of 7.5 MPa·m$^{1/2}$, then dropped to 6.0 ± 0.2 MPa·m$^{1/2}$ for the uniaxial spiral lengths.

The average fracture toughness was 6.1 ± 0.2 MPa·m$^{1/2}$, an increase of ~45%.

Table II. Mechanical Properties

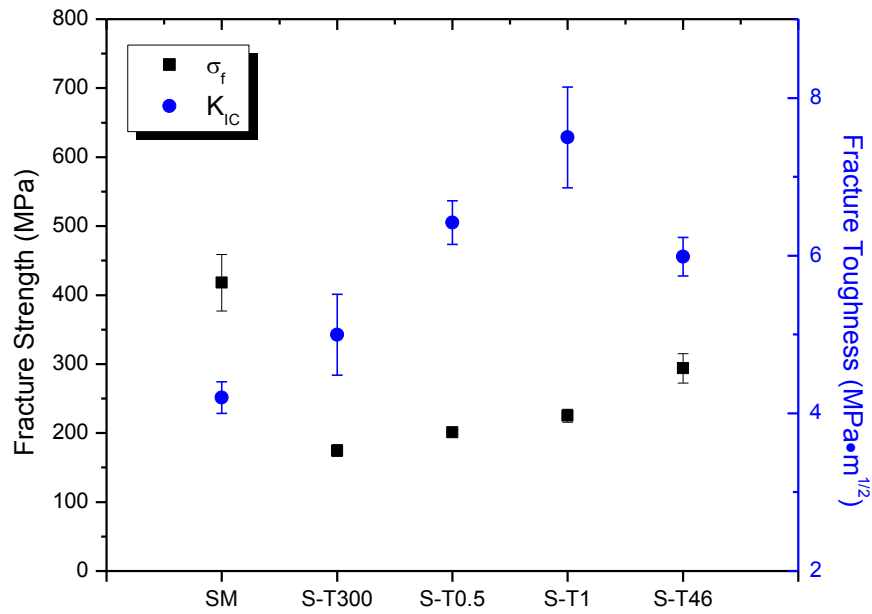| Specimen ID	Relative Density	Flexure Strength (MPa)			Fracture Toughness (MPa·m$^{1/2}$)		
SM	98%	418	±	41	3.8	±	0.6
S-T300	97%	175	±	8.3	4.4	±	0.4
S-T0.5	98%	201	±	4	6.4	±	0.3
S-T1	97%	225	±	9.3	7.5	±	0.6
S-T46	98%	294	±	21	6.0	±	0.2

Figure 3. Fracture strength and toughness of SiC - TiB$_2$ specimens in order of increasing spiral length.

Optical micrographs of Vickers indents in Figure 4 show the crack deflection caused by the addition of spirals in the matrix, increasing the fracture toughness. Image (a) illustrates what a typical indent for a direct crack fracture toughness measurement should look like. Image (b) consists of an indent in close proximity to two spirals. The radial cracks protrude from the tips of the indent as expected; however, due to residual stresses in the matrix, the cracks curve and deflect away from the spiral additions. Most notably in image (c) of the uniaxial sample, the radial cracks parallel to the spirals extend laterally as they do in image (a); though the radial cracks perpendicular to the spiral orientation are deflected as the fracture energy is absorbed in the microcracking present in the spiral layers. Image (d) is an indent placed in the middle of the TiB_2 spiral. The indent geometry cannot be distinguished from the amount of spalling in the TiB_2, though it should be noted that none of the radial/median cracks from the indent extend past the outermost layer of the spiral.
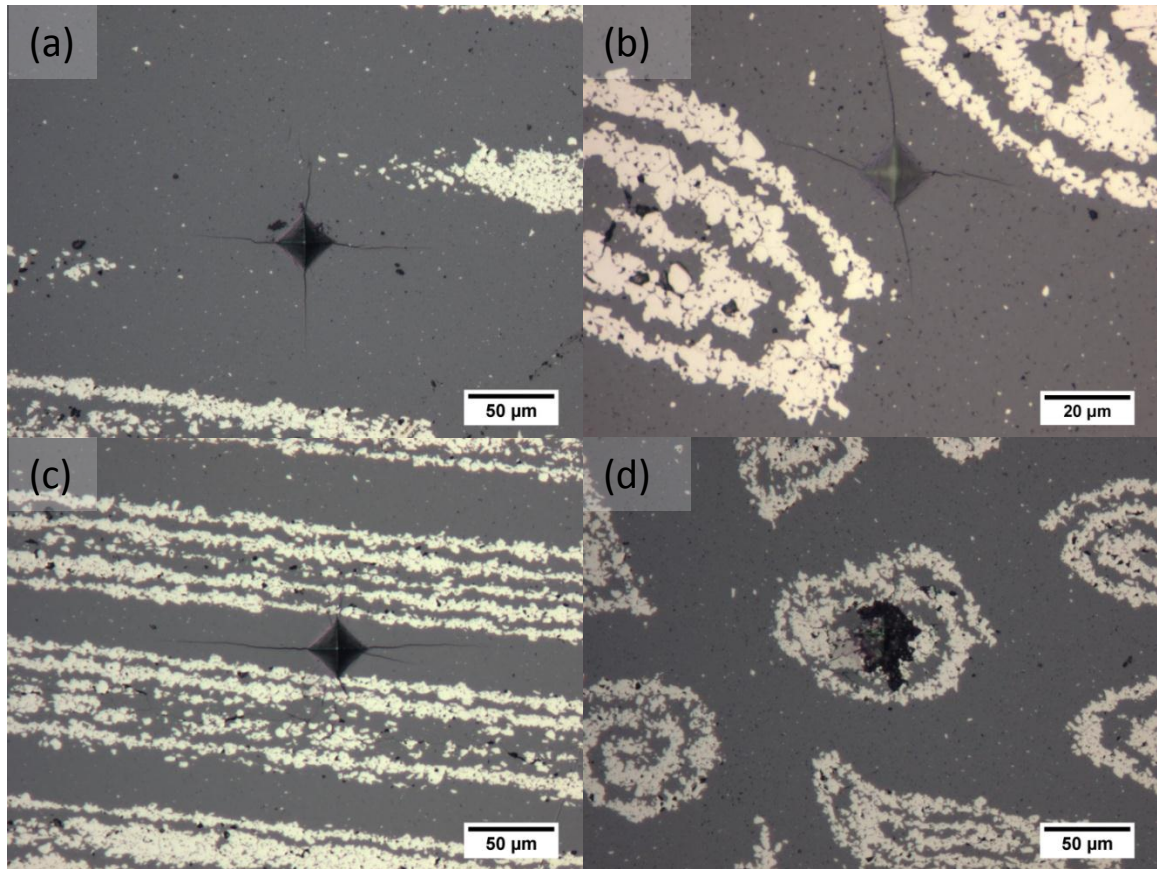
Figure 4. Fracture toughness indents (a) within a spiral, (b) near spirals with residual stresses, (c) between uniaxial spirals, and (d) in SiC matrix

Utilizing the data from mechanical properties, the critical flaw size (c) was calculated with Equation 1 using the Griffith criteria assuming the crack geometry follows a semicircular, penny, shape where Y=2/√π.

$$c = \left(\frac{K_{IC}}{\sigma_f Y}\right)^2 \tag{1}$$

The calculated critical flaw sizes are plotted in Figure 6 with respect to the spiral geometry. The uniaxial spiral geometry had the smallest c of 325 µm, whereas the 1 mm long spirals resulted in a maximum c of 872 µm. The critical flaw size for the randomly oriented 300 µm and 0.5 mm spiral lengths correlate with approximately twice the spiral

length. It could be proposed based on this observation that two of the randomly oriented spirals filaments oriented such that the microcracking was able to continue through two filament lengths, increasing c.

For wear testing, the uniaxial and monolithic compositions from the study were chosen to move forward with characterization of the wear behavior. The uniaxial specimen was chosen due to its high strength relative to the other spiral compositions and increased fracture toughness over the monolithic composition. The wear testing conducted following ASTM G65 resulted in minimal wear scars, with volume losses for the monolithic and uniaxial spiral specimens approximately $1.8 \cdot 10^{-4}$ mm^3 rev^{-1} and $5.5 \cdot 10^{-4}$ mm^3 rev^{-1}, respectively (Table III and Figure 7). Cross-sections, illustrated in Figure 5, of the wear scar indicate a uniform wear across the surface of the monolithic specimen (c and d); however, in the uniaxial sample (a and b), preferential wear of the spiral regions was observed with the SiC matrix wearing slower, resulting in a wave-like pattern, most evident in c. Images a and b are towards the edge of the wear scar where there is less force on the sample and b and d near the center, where the 30 lb force was at its maximum. The depth of the wave-like pattern was maximum in this area, with almost negligible wave depth near the center, evident in image b.
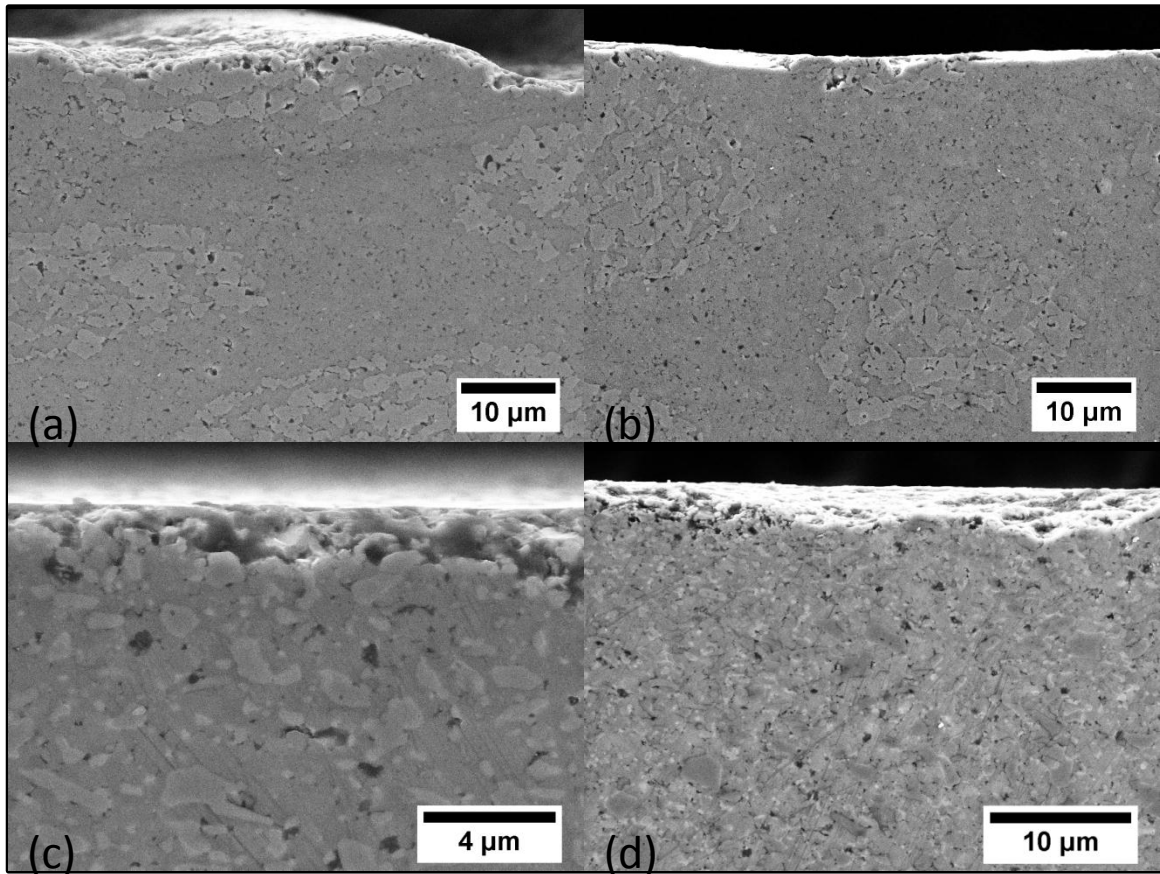
Figure 5. SEM images of wear scar cross-sections of the uniaxial sample, (a) and (b), and the monolithic, (c) and (d). Images (b) and (d) are towards the center of the wear scar, whereas (a) and (c) are towards the edge of the wear scar.

Flexure testing of the composites as well as the monolith post wear testing was performed in an effort to better understand surface damage affected their mechanical properties (a minimum of 3 bars were tested for each set). Results of specimen 4-pt flexure after wear testing are illustrated in Figure 8 and tabulated in Table III. As a result of wear testing, the monolithic sample had an 18% lower strength than the as ground surface of the same original billet whereas the uniaxial specimen increased in strength by 16%. Examination of the wear scar cross-sections did not reveal a significant

difference in sub surface damage in the monolithic surface, though when compared to polished flexure strength bars in the initial portion of the study, they are approximately the same, especially considering the standard deviations. King[16] also observed higher strength of the as-ground to 600 grit 4-pt bend specimens in comparison to those specimens polished to 0.25 μm.

It can be proposed that the increased strength of the uniaxial spiral samples is due to preferential wear of the microcracked spirals. If the flaws are recessed into the sample, thus under reduced tension in flexure, the strength would more dependent on that of the matrix material.
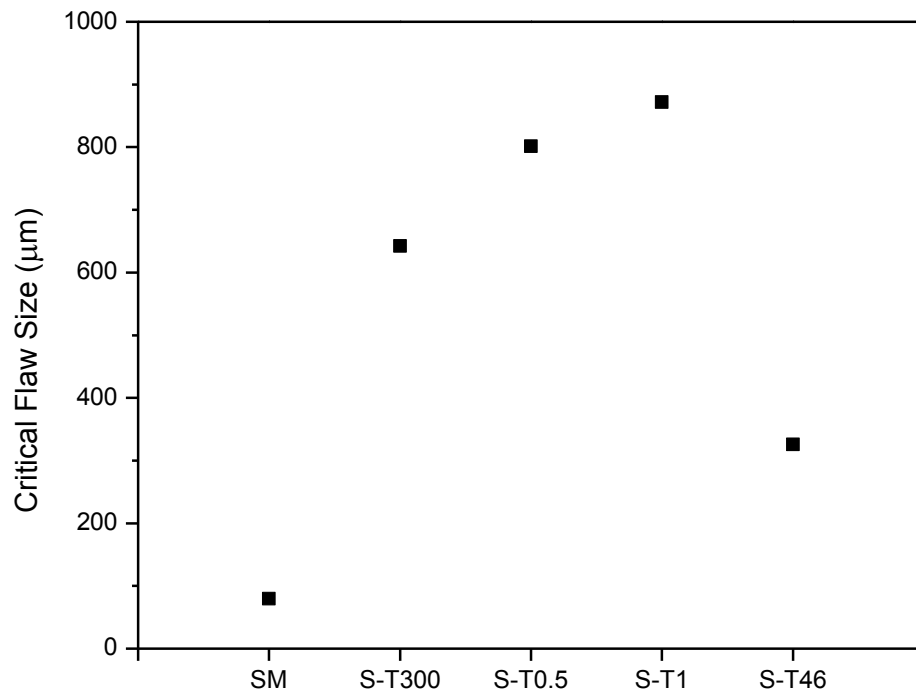
Figure 6. Calculated critical flaw size using Griffith criteria assuming $Y = 2/\sqrt{\pi}$

Table III. Wear Testing Results

Specimen ID	Average Wear Loss (mm^3)			Flexure Strength Post- Wear (MPa)			Flexure Strength As-Ground (MPa)		
SM	1.1	±	0.6	405	±	28	494	±	36
S-T46	3.3	±	0.6	320	±	20	275	±	38
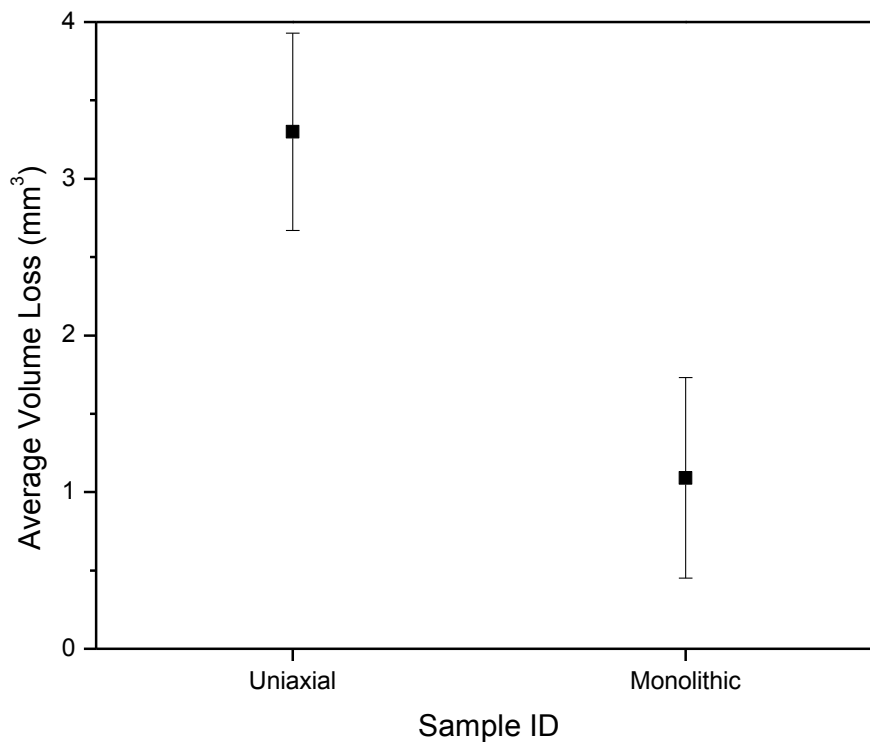
Figure 7. Average volume loss for uniaxial and monolithic samples after ASTM G65 Procedure A.
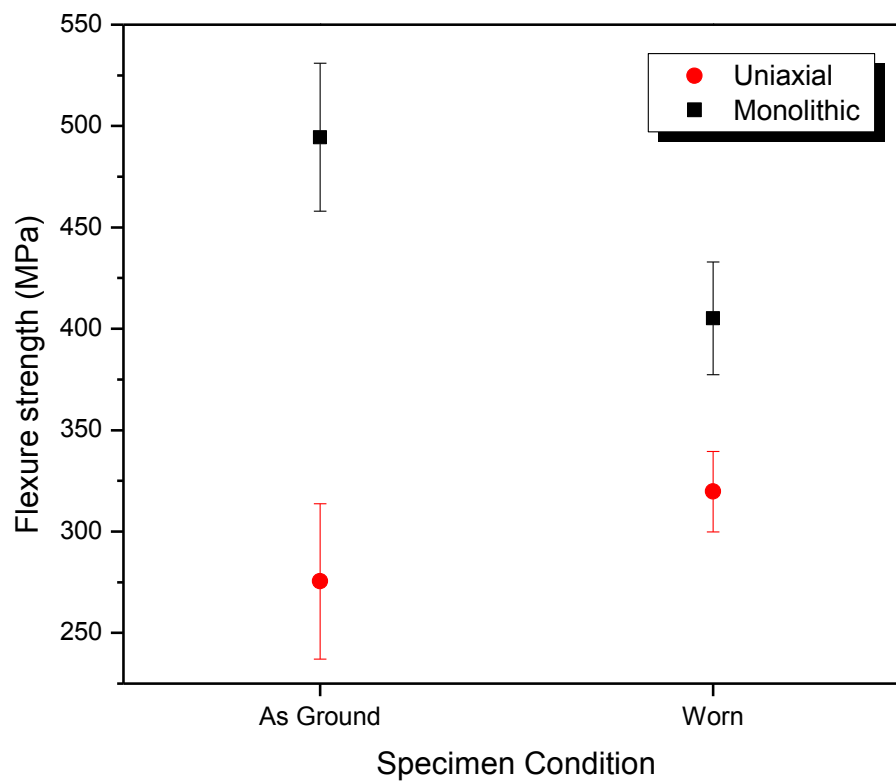
Figure 8. Flexure strength of uniaxial and monolithic samples as surface ground with 600 grit diamond wheel and after undergoing wear testing following ASTM G65.

CONCLUSIONS

TiB$_2$ spiral additions, ~50 μm in diameter, were incorporated into a SiC matrix at a nominal 25 vol% with varying spiral lengths. The addition of the spirals resulted in a 46% decrease in strength with an average strength of 224 MPa in comparison to the 418 MPa exhibited by the monolithic composition. The maximum strength from the spiral additions was 294 ± 21 MPa exhibited by the uniaxial sample (spirals spanning the full length of the test specimens). The average fracture toughness increased ~45% with the

greatest toughness exhibited by the 1 mm spiral length at 7.5 MPa·m$^{1/2}$. The critical flaw

size was calculated using Griffith criteria and correlated well with twice the length of the

randomly oriented spiral lengths. With respect to the wear testing, the monolithic

composition exhibited less wear than the uniaxial specimen 1.1 mm^3 and 3.3 mm^3 per

6,000 revolutions, respectively. However, the uniaxial spirals exhibited a post-wear

strength increase of 16%; whereas the monolithic exhibited a reduced strength of 18%

after wear testing.

ACKNOWLEDGEMENTS

REFERENCES

1.　　Munro RG "Material Properties of a Sintered α-SiC" J. Phys. Chem. Ref. Data. **26**　[5] (1997)

2.　　Flinders M, Ray D, Anderson A, and Cutler R.A, "High-Toughness Silicon Carbide as Armor," J. Am. Ceram. Soc., **88** [8] 2217–26 (2005)

3.　　Schneider SJ Jr., Engineered Materials Handbook: Ceramics and Glasses. Vol. 4, ASM International, Materials Park, OH, 1991

4.　　Luo Z, Zhou X, Yu J, "Mechanical properties of SiC/SiC composites by PIP process with a new precursor at elevated temperature" Mat'l Sci & Eng A 607 (2014) 155-61

5.　　King DS, Fahrenholtz WG, Hilmas GE. Silicon carbide-titanium diboride ceramic composites. Journal of the European Ceramic Society. 2013;33(15-16):2943-51

6.　　Cho K, Choi H, Lee J, Kim Y. In situ enhancement of toughness of SiC-TiB2 composites. J Mater Sci. 1998;33(1):211-4.

7.　　Kamiya A, Nakano K, Kondoh A, "Fabrication and properties of hot-pressed SiC whisker-reinforced TiB2 and TiC composites." J. of Mat'l. Sci. Letters **8** 566-568 (1989)

8.　　Fei J, Wang W, Ren A, Ji Y, Zhou J, Zhu M. Mechanical properties and densification of short carbon fiber-reinforced TiB2/C composites produced by hot pressing

9.　　Watts J, Hilmas G, Fahrenholtz W, "Mechanical Characterization of ZrB2-SiC Composites with Varying SiC Particle Sizes" J. Am. Ceram. Soc. **94** [12] 4410-18

10.　　Magley D, Winholtz F, Faber K, "Residual Stresses in a Two-Phase Microcracking Ceramic" J. Am. Cera. Soc. **73** [6] 1641-4 (1990)

11.　　Teague M, "Modeing and Measurement of Thermal Residual Stresses and Isotope Effects on Thermo Physical Properties of ZrB2-SiC Ceramics," Materials Sience and Engineering, Missouri University of Science and Technology, Master of Science, 2008

12.　　Watts J, Hilmas G, Fahrenholtz W, "A Method for Toughening via the Production of Spiral Architectures Through Powder Loaded Polymer Extrusion and Toughened Materials Formed Thereby," United States Patent, 8,192,853, 2012

13.　　Els A, Watts J, Hilmas G, Fahrenholtz W, "Processing and Properties of TiB2-SiC and TiB2-SiC/BN Ceramics Containing a Spiral Architecture" To be submitted 2014

14.　　ASTM International, "Standard Test Method for Flexural Strength of Advanced Ceramics at Ambient Temperature" ASTM Standard C1161-02c, West Conshohocken, PA.

15.　　Buckholz S, "The Influence of Aluminum and Carbon on the Abrasion Resistance of High Manganese Steels," Missouri University of Science and Technology, Master of Science, 2013.

16.　　King D, "Microstructure and Mechanical Properties of Silicon Carbide-Titanium Diboride Ceramic Composites" Missouri University of Science and Technology, Master of Science, 2012.

SECTION

3. SUMMARY AND CONCLUSIONS

3.1 SUMMARY OF RESULTS

The addition of ceramic spirals in a ceramic composite was studied. Two studies were presented in this manuscript. Paper I focused on the formation of a consistent spiral and measuring the mechanical properties to determine the spiral addition's effects. Conclusions in regards to critical flaw size were not able to be made due to the microcracking present in the TiB_2 matrix. Paper II focused on a better designed experiment with determining the critical flaw size of the co-extruded spiral materials. Spirals of the same multi-filament co-extrusion method were chopped to different lengths as well as a randomly oriented 300 µm single filament co-extrusion filament 300 µm in length. In this section, each paper is summarized followed by overall conclusions from the present work.

3.1.1 Paper I. Co-extrusion techniques were modified in order to consistently fabricate a SiC spiral microstructure in a TiB_2 matrix. The SiC spiral size was minimized to a diameter of ~50 µm, achieved by a MFCX of 2.4 mm/1 mm. Smaller extrusions resulted in an inconsistent spiral microstructure due to particle size limitations. The average fracture strength of the spiral architectures was 193 MPa which was a 60%

reduction when compared to the particulate composite strength of 488 MPa. The fracture toughness on the other hand increased by ~40% on average with a maximum fracture toughness of 8.2 MPa·m$^{1/2}$. Critical flaw size was calculated from experimental values and correlated with the filament diameter; however, the microcracking in the matrix must be resolved before making this conclusion.

3.1.2 Paper II. TiB$_2$ spirals were incorporated into a SiC matrix extruded to a ~50 μm diameter via 2.4 mm/1 mm MFCX. The lengths of the spiral additions were altered to determine the relation of the critical flaw size to the spiral addition. The addition of spirals resulted in a 46% decrease in strength, but a 45% increase in toughness with a maximum fracture toughness of 7.5 MPa·m1/2 exhibited by the 1 mm long randomly oriented spiral. The calculated critical flaw size correlates with twice the oriented spiral length for the shorter spirals lengths, and the length of a single filament for the 1 mm randomly oriented sample. The volume loss after wear testing of the uniaxial spirals was greater than that of the particulate composite, 3.3 mm^3 and 1.1 mm^3, respectively. The wear scars of the uniaxial sample indicated preferential wear of the TiB$_2$ spiral phase. When tested in flexure with the wear scar in tension, the uniaxial spiral samples exhibited an increase in strength whereas the monolithic resulted in a decrease in strength in comparison to the as ground equivalent.

3.2 OVERALL CONCLUSIONS

Overall, this research modified the co-extrusion technique to create novel geometries in a matrix that are not axisymmetric or co-axial. The research focused on producing a consistent microstructure and characterizing the mechanical properties. Some of the overall conclusions that can be made from the studies described in this manuscript are as follows:

- Multi-filament co-extrusion can be used to produce a consistent spiral microstructure

- With the starting powders used in this research, a 50 µm diameter spiral is the smallest that can be achieved before encountering particle size limitations

- The residual stresses induced by the thermal expansion mismatch of TiB_2 and SiC are too significant to be overcome with small compositional changes

- The tradeoff between strength and fracture toughness in ceramics was observed in each study. Study II at a near even tradeoff of ~45%

- Fracture toughness increased in both studies I and II conducted by 40% and 45%, respectively

- Post-wear strengths of the uniaxial spiral composition exceeded that of the as-ground samples whereas the monolithic sample decreased in strength.

4. FUTURE WORK

In this research, a multi-filament co-extrusion procedure of extruding with 2.4 mm spinneret to 1 mm spinneret, resulted in the most consistent spiral microstructure without particle size being a limiting factor. However, if the particle sizes were reduced, smaller spiral additions could then be fabricated, reducing the size of the inclusion. This may result in an increased strength value.

The calculated flaw sizes from this research assume a crack geometry using Griffith's criteria. In order to better understand the failure mechanisms in the spiral materials, fractography should be done to analyze the fracture surfaces to determine where the crack is originating from. This would be beneficial in determining the critical flaw, thus possibly linking it to an extrusion or processing parameter that can be improved upon in the future.

The wear results from ASTM G65 caused minimal amounts of wear on the SiC-25 vol% TiB_2 sample. To better understand the wear behavior of the materials studied, a high shear wear test, pin-on-disk for example, should be tested to better understand the wear mechanisms of the materials and determine if the wear observed in this study is consistent with that in a high shear setting. In addition, the strength post-wear should also be measured to be compared with the findings in this study.

It is also advised to utilize the EDM on the S&T campus to cut a machining tip from the studied material to test in machining applications.

REFERENCES

1.   Munro RG "Material Properties of a Sintered α-SiC" J. Phys. Chem. Ref. Data. **26** [5] (1997)

2.   Munro RG. Material properties of titanium diboride. Journal of Research of the National Institute of Standards and Technology. **105** [5] 709-20 (2000)

3.   King D, Fahrenholtz W, Hilmas G. Silicon carbide-titanium diboride ceramic composites. Journal of the European Ceramic Society. 2013;33(15-16):2943-51

4.   Cho K, Choi H, Lee J, Kim Y. In situ enhancement of toughness of SiC-TiB2 composites. J Mater Sci. 1998;33(1):211-4.

5.   Kamiya A, Nakano K, Kondoh A, "Fabrication and properties of hot-pressed SiC whisker-reinforced TiB2 and TiC composites." J. of Mat'l. Sci. Letters **8** 566-568 (1989)

6.   Fei J, Wang W, Ren A, Ji Y, Zhou J, Zhu M. Mechanical properties and densification of short carbon fiber-reinforced TiB2/C composites produced by hot pressing

7.   Popovic' D, Halloran J, Hilmas GE, Brady GA, Somers S, Barda A, Zywicki G, "Process for Preparing Textured Ceramic Composites", U.S. Patent No. 5,645,781

8.   Teague M, "Modeing and Measurement of Thermal Residual Stresses and Isotope Effects on Thermo Physical Properties of ZrB2-SiC Ceramics," Materials Sience and Engineering, Missouri University of Science and Technology, Master of Science, 2008

9.   Watts J, Hilmas G, Fahrenholtz W, "A Method for Toughening via the Production of Spiral Architectures Through Powder Loaded Polymer Extrusion and Toughened Materials Formed Thereby," United States Patent, 8,192,853, 2012

10.   Anderson TL. *Fracture Mechanics: Fundamentals and Applications, Third Edition*. Taylor & Francis Group. 26 (2003)

11.   Wachtman J, Cannon W, Matthewson M, Mechanical Properties of Ceramics. Second Edition. John Wiley & Sons, Inc. 68 (2009)

12.   ASTM International, "Standard Test Method for Flexural Strength of Advanced Ceramics at Ambient Temperature" ASTM Standard C1161-02c, West Conshohocken, PA.

13.   Green DJ, An Introduction to the Mechanical Properties of Ceramics. 1998. Cambridge University Press.

14.   ASTM International "Standard Test Methods for Determination of Fracture Toughness of Advanced Ceramics at Ambient Temperature" ASTM Standard C1421-10. West Conshohocken, PA

15.   Coblenz, W.S., "Fibrous Monolithic Ceramic and Method for Production", U.S. Patent No. 4,772,524

16.   Baskaran S, Nunn S, Popovic D, Halloran J, "Fibrous Monolithic Ceramic: I, Fabrication, Microstructure, and Indentation Behavior", J. Am. Ceram. Soc., 76 [9] 2209-2216 (1993)

17.   Hilmas G, Brady G, Halloran J. "SiC and Si3N4 Fibrous Monoliths: Nonbrittle Fracture from Powder-Processed Ceramics Produced by Coextrusion" **51** Fifth International Conference on Ceramic Processing Science and Technology. 609-14 (1994)

18.   Watts J, "Development and Characterization of Tungsten Carbide Based Composites," Ceramic Engineering , University of Missouri – Rolla, Master of Science, 2004.

19.   Zimmermann J, Hilmas G, Fahrenholtz W, "Thermal Shock Resistance and Fracture Behavior of ZrB2-Based Fibrous Monolith Ceramics" J. Am. Ceram. Soc. **92** [1] 161-166 (2009)

20.   He M, Hutchinson J, "Crack Deflection at an Interface between Dissimilar Elastic Materials," Int. J. Solids Struct., 25 [9] 1053-67 (1989)

21.   S. Baskaran, J. Halloran, "Fibrous Monolithic Ceramics: III, Mechanical Properties and Oxidation Behavior of the Silicon Carbide/Boron Nitride System", *Journal of the American Ceramic Society,* Vol. 77. No. 5, pp. 1249-1255 (1994)

22.   S. Baskaran, S. Nunn, J. Halloran, "Fibrous Monolithic Ceramics: IV, Mechanical Properties and Oxidation Behavior of the Alumina/Nickel System", *Journal of the American Ceramic Society,* Vol. 77, No. 5, pp. 1256-1262 (1994)

23.   Basu B, Processing and properties of monolithic TiB2 based materials. Int Mater Rev 2006; **51**(6):352-74

24.   Baik S, Becher PF. "Effect of Oxygen Contamination on Densification of TiB2" J. Am. Ceram. Soc. **70** [8] 527-30 (1987)

25.   Prochazka S, Scanlan, RM. "Effect of Boron and Carbon on Sintering of SiC" J. Am. Ceram. Soc. **58** [1-2] 72 (1974)

26.   Greskovich C, Rosolowski JH. "Sintering of Covalent Solids" J. Am. Ceram. Soc. **59** [7-8] 336-343 (1976)

27.   DeJonghe L, Rahaman M, "Sintering of Ceramics" Handbook of Advanced Ceramics. Elsevier. 191 (2003)

28.   Kang E, Jang C, Lee C, Kim C. "Effect of Iron and Boron Carbide on the Densification and Mechanical Properties of Titanium Diboride Ceramics" J. Am. Ceram. Soc **72** [10]1868-72 (1989)

29.   R. A. Cutler, "Engineering Properties of Borides," pp. 787-803. in Ceramics and Glasses, Engineered Materials Handbook*,* **4** Edited by S. J. Schneider Jr. ASM International, Materials Park, OH, 1991.

30.   Ferber MK, Becher PF, Finch CB. Effect of microstructure on the properties of TiB2 ceramics. *J Am Ceram Soc* 1983;**66**(1):C-2–3.

31.   Munro RG. Material properties of titanium diboride. Journal of Research of the National Institute of Standards and Technology. **105** [5] 709-20 (2000)

32.   King DS, Fahrenholtz WG, Hilmas GE. Silicon carbide-titanium diboride ceramic composites. Journal of the European Ceramic Society. 2013;33(15-16):2943-51

33.   Munro RG "Material Properties of a Sintered α-SiC" J. Phys. Chem. Ref. Data. **26** [5] (1997)

34.   Flinders M, Ray D, Anderson A, and Cutler R.A, "High-Toughness Silicon Carbide as Armor," J. Am. Ceram. Soc., **88** [8] 2217‑26 (2005)

35.   Schneider SJ Jr., Engineered Materials Handbook: Ceramics and Glasses. Vol. 4, ASM International, Materials Park, OH, 1991

36.   Chen Y, Jiang L, Jia X. Properties of pressureless sintered SiC-TiB2 composites. Advanced Materials Research, 177, 369 (2010)

37.   Cho K, Choi H, Lee J, Kim Y. In situ enhancement of toughness of SiC-TiB2 composites. J Mater Sci.**33** [1] 211-4 (1998).

VITA

Andrea Lynn Els was born December 1, 1989 in St. Charles, Missouri; growing up in Hermann, MO. In May 2012 she received her Bachelor of Science degree in Ceramic Engineering at Missouri University of Science and Technology. During her undergraduate career, Andrea was active in leadership roles within Material Advantage and Keramos in addition to being an undergraduate research assistant from 2010 until graduation. In addition she held a summer internship position at Vesuvius USA in 2011.

Andrea began her master's program in Aerospace Engineering with the hopes of broadening her knowledge. However, due to complications and realization that materials science was her passion, she returned to the Materials Science & Engineering Department. She began her new master's project with Dr. Jeremy Watts in September 2012. During her time as a master's student, Andrea was a graduate teaching assistant for the Sintering and Microstructure Development laboratory as well as working in the Sports Information Department. Andrea earned her Master of Science degree in Materials Science & Engineering in August 2014. She will continue her materials engineering career with Corning Incorporated - Environmental Technologies Division in Erwin, NY.